Naturwissenschaften (2006) 93:519–542
DOI 10.1007/s00114-006-0138-6

REVIEW

Changes in earth's dipole

Peter Olson · Hagay Amit

Received: 14 July 2005 / Revised: 11 May 2006 / Accepted: 18 May 2006 / Published online: 17 August 2006

Abstract The dipole moment of Earth's magnetic field has decreased by nearly 9% over the past 150 years and by about 30% over the past 2,000 years according to archeomagnetic measurements. Here, we explore the causes and the implications of this rapid change. Maps of the geomagnetic field on the core–mantle boundary derived from ground-based and satellite measurements reveal that most of the present episode of dipole moment decrease originates in the southern hemisphere. Weakening and equatorward advection of normal polarity magnetic field by the core flow, combined with proliferation and growth of regions where the magnetic polarity is reversed, are reducing the dipole moment on the core–mantle boundary. Growth of these reversed flux regions has occurred over the past century or longer and is associated with the expansion of the South Atlantic Anomaly, a low-intensity region in the geomagnetic field that presents a radiation hazard at satellite altitudes. We address the speculation that the present episode of dipole moment decrease is a precursor to the next geomagnetic polarity reversal. The paleomagnetic record contains a broad spectrum of dipole moment fluctuations with polarity reversals typically occurring during dipole moment lows. However, the dipole moment is stronger today than its long time average, indicating that polarity reversal is not likely unless the current episode of moment decrease continues for a thousand years or more.

Keywords Dipole moment · Earth · Magnetic field · Core–mantle boundary · South Atlantic Anomaly

P. Olson (✉) · H. Amit
Department of Earth and Planetary Sciences,
Johns Hopkins University,
Baltimore, MD, USA
e-mail: olson@jhu.edu

Introduction

The main part of the geomagnetic field originates in the Earth's iron-rich, electrically conducting, molten outer core. The outer core is in a state of convective overturn, owing to heat loss to the solid mantle, combined with crystallization and chemical differentiation at its boundary with the solid inner core. The geodynamo is a byproduct of this convection, a dynamical process that continually converts the kinetic energy of the fluid motion into magnetic energy (see Roberts and Glatzmaier 2000; Buffett 2000; Busse 2000; Dormy et al. 2000; Glatzmaier 2002; Kono and Roberts 2002; Busse et al. 2003; Glatzmaier and Olson 2005 for the recent progress on convection in the core and geodynamo).

According to the dynamo theory the geomagnetic field has a complex structure within the core. But this dynamo-generated field, often called the *core field*, is relatively simple near the Earth's surface, consisting of a dipole slightly inclined to the rotation axis that accounts for about 80% of the total and a weaker nondipole part that accounts for the remainder (Langel et al. 1980; Olsen et al. 2000). When the core field is time-averaged over intervals of several centuries or longer, the nondipole part tends to vanish, leaving a field that consists almost entirely of an inclined geocentric dipole, as illustrated in Fig. 1. The inclination (or tilt) of the dipole, the primary deviation from rotational symmetry in the core field, is also a transient property, although time averages over several millennia are needed to remove its effects (Carlut et al. 2000). What remains of the core field once the tilt and nondipole components are averaged out is nearly a geocentric axial dipole, an important reference state that is abbreviated GAD.

The tendency toward the GAD configuration is a defining property of the geomagnetic field, both in the recent past and through most of Earth's history. It is estimated that the

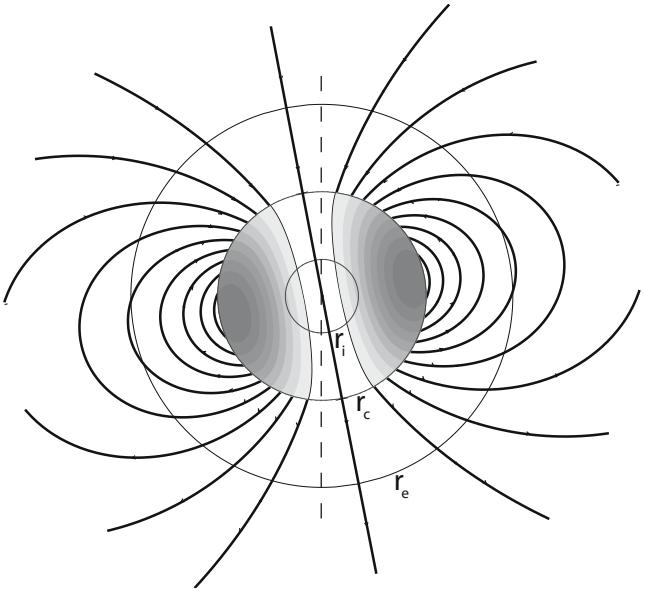

Fig. 1 Idealized cross-section of the Earth showing an inclined dipole magnetic field maintained by the slowest decaying (fundamental mode) electric current distribution in the core. $r_e = 6371\ km$, $r_c = 3480\ km$, and $r_i = 1221\ km$ denote surface, core–mantle boundary, and inner–outer core radii, respectively. The solid mantle and crust ($r > r_c$) are poor electrical conductors. The liquid outer core ($r < r_c$) and solid inner core are electrically conducting, iron-rich alloys. Field *lines* show the present-day (normal) geomagnetic dipole polarity and its inclination or tilt (10.3°). *Filled contours* represent density of azimuthal (east–west) electric currents with shading proportional to negative (west-directed) current density

5 Ma time-averaged field is about 95% GAD (Johnson and Constable 1997; Carlut and Courtillot 1998), and the 120 Ma average field is comparably dipolar (Livermore et al. 1984). Paleomagnetic evidence indicates that the main departure from the GAD configuration in the time-averaged field consists of a small axial quadrupole. There is additional paleomagnetic evidence suggesting there may also be small nonaxial, higher order multipoles in the time-averaged field, although the precise composition of these terms is not agreed on (Dormy et al. 2000). No vestige of when the geodynamo began was found in the geologic record. The magnetization of ancient rocks indicates the Earth had a magnetic field and an active dynamo as early as 3.5 Ga (Hale and Dunlop 1987; Yoshihara and Hamano 2000). Most theoretical studies of the early Earth conclude that the geodynamo began to operate during or shortly after the formation of the core (Stevenson 1990), which is estimated to have taken place around 4.5 Ga (Wood and Halliday 2005).

In spite of its remarkable persistence, the geomagnetic dipole is continually changing, sometimes dramatically. Polarity reversals are probably the best-known example of rapid dipole changes. The geomagnetic field is known to have reversed its polarity hundreds of times in the geologic past (295 reversals were identified in the 160 Ma marine magnetic anomaly record alone), and there is a comparable number of instances where the field has made large amplitude, transient deviations from the GAD configuration called excursions (Gubbins 1999; Merrill and McFadden 1999; Constable 2003). In addition to directional changes, the strength of the dipole is also variable. In our own time, we are witnessing a precipitous drop in the dipole moment, which we describe more fully in the following section.

The particular combination of long-term steadiness and short-term fluctuations of the dipole raises fundamental questions about the core and the geodynamo. Why does the core field tend toward an axial dipole? Are there significant long-term departures from GAD? What controls the dipole moment strength and why does it fluctuate? What causes polarity reversals? Is today's dipole moment decrease a precursor of a more fundamental change, such as a polarity reversal? Answers to these questions would have both practical and scientific benefits. In this review, we focus on one of these issues, the origin of the present-day rapid decrease in the dipole moment. We begin by describing the present-day dipole moment change and compare it with theoretical rates for Ohmic decay of dipole fields in the core. We then summarize the evidence for dipole moment changes on historical (centennial), archeomagnetic (millennial), and paleomagnetic (geological) time scales. We analyze the structure of the present-day geomagnetic field and its secular variation on the core–mantle boundary, delineating the places where today's rapid drop in the geomagnetic dipole moment is occurring. The sources of the South Atlantic Anomaly (SAA), a region of the external field with low magnetic intensity that has attracted recent attention as a space radiation hazard, are identified with some of these locations on the core–mantle boundary. We discuss some consequences of a weakened geomagnetic dipole moment, particularly for manned and unmanned travel in space. We quantify some of the dynamo mechanisms responsible for the observed moment change and show that these similar mechanisms cause rapid dipole moment drops in numerical dynamo models. Lastly, we project our results into the future. We argue that the present state of the field at the core–mantle boundary and the persistence of certain large-scale flow structures just below the core–mantle boundary indicate that the dipole moment will continue to decrease for some time, although the prospect of this being a prelude to full polarity reversal is remote.

The dipole moment and the core field

Figure 1 shows the basic spherically symmetric structure of the Earth's interior, including the metallic core, the

solid silicate and oxide mantle, and the crust. The core is subdivided into the liquid outer core and the solid inner core. According to the seismic Preliminary Reference Earth Model (Dziewonski and Anderson 1981), the mean spherical radii of the surface, core–mantle boundary, and inner–outer core boundary are $r_e = 6371$, $r_c = 3480$, and $r_i = 1221\ km$, respectively. Figure 1 also shows an inclined, fundamental mode dipolar magnetic field originating from an idealized distribution of azimuthal electric currents in the core.

The internal origin of Earth's dipole was first established by Gauss (1877) and it is now accepted that its source consists almost entirely of free electric currents within the core. The silicates and oxides that make up the mantle and crust are very poor electrical conductors in comparison with the iron-rich core alloys (see Stacey 1992 for a general discussion of the electrical conductivity structure of the Earth) and for purposes of this review the mantle and crust can be considered as insulators. A possibly important exception is the D''-region, a 50- to 200-km-thick layer at the base of the mantle just above the core–mantle boundary. Some properties of the D''-region differ significantly from the rest of the lower mantle (Schubert et al. 2001; Murakami et al. 2004) and, in particular, there is evidence it may have a higher electrical conductivity (Buffett 1992). However, the D''-layer does not appear to have much effect on the dipole moment. Ferromagnetism is limited to shallow depths in the crust and is also spatially heterogeneous, so it contributes little to the dipole and other large-scale components of the field (Cain et al. 1989; Maus et al. 2002, 2005; Sabaka et al. 2002, 2004). By restricting attention to the long wavelength part of the geomagnetic field, regularized inversion methods combined with potential theory (Gubbins 2004) allow downward continuation of surface and satellite magnetic measurements through the crust and mantle, all the way to the core–mantle boundary. Further downward continuation of the surface field is not possible because of the presence of electric currents in the core, but at least we can image the large-scale part of the field as it emerges from the core.

Above the core–mantle boundary, the standard representation of the geomagnetic field **B** (SI unit: Tessla) is as a potential field satisfying $\mathbf{B} = -\nabla\Psi$ in which the geomagnetic potential Ψ has the following definition:

$$\Psi = r_e \sum_{l=1}^{\infty} \sum_{m=0}^{l} \left(\frac{r_e}{r}\right)^{l+1} P_l^m(\cos\theta)\left(g_l^m \cos m\phi + h_l^m \sin m\phi\right) \tag{1}$$

where (r, θ, ϕ) are geocentric spherical coordinates (radius, colatitude, and east longitude, respectively), P_l^m are the Schmidt-normalized associated Legendre polynomials, and g_l^m and h_l^m are the Gauss coefficients of degree l and order m (Chapman and Bartels 1962; Backus et al. 1996). The geomagnetic dipole moment vector **m** can be expressed in terms of the radial component of the geomagnetic field B_r, or in terms of the degree $l = 1$ coefficients in Eq. 1 as:

$$\begin{aligned} \mathbf{m} &\equiv (\mathrm{m_x}\hat{\mathbf{x}} + \mathrm{m_y}\hat{\mathbf{y}} + \mathrm{m_z}\hat{\mathbf{z}}) \\ &= \frac{3\mathrm{r}}{2\mu_0} \int \mathrm{B_r}(\sin\theta\cos\phi\hat{\mathbf{x}} + \sin\theta\sin\phi\hat{\mathbf{y}} + \cos\theta\hat{\mathbf{z}})\mathrm{dS} \\ &= \frac{4\pi \mathrm{r_e^3}}{\mu_0}(\mathrm{g_1^1}\hat{\mathbf{x}} + \mathrm{h_1^1}\hat{\mathbf{y}} + \mathrm{g_1^0}\hat{\mathbf{z}}) \end{aligned} \tag{2}$$

where $(\hat{\mathbf{x}}, \hat{\mathbf{y}}, \hat{\mathbf{z}})$ are Cartesian unit vectors with origin at Earth's center (z is the polar axis, x and y are axes in the equatorial plane with x through 0° longitude and y through 90° East longitude), (m_x, m_y, m_z) are the dipole moment components along these axes, $\mu_0 = 4\pi \times 10^{-7}\ Hm^{-1}$ is the free space magnetic permeability, dS denotes surface integration over a sphere with radius r, and g_1^0 and (g_1^1, h_1^1) are the axial and equatorial dipole Gauss coefficients, respectively. As defined in Eq. 2, **m** has units Am^2 (Ampere meter-squared).

The Ørsted satellite measurements give $g_1^0 = -29617.37$, $g_1^1 = -1729.24$, and $h_1^1 = 5185.65\ nT$ (nano-Tessla) for the core field at epoch 2000 (Olsen et al. 2000). According to these values, the axial moment was $m_z = -7.66 \times 10^{22}\ Am^2$ at epoch 2000, and the components of the equatorial moment were $m_x = -0.447 \times 10^{22}$ and $m_y = 1.34 \times 10^{22}\ Am^2$ at the same time. Therefore, the strength of the dipole moment at 2000 was $|\mathbf{m}| \equiv \sqrt{(\mathrm{m_x^2} + \mathrm{m_y^2} + \mathrm{m_z^2})} = 7.79 \times 10^{22}\ Am^2$ and the so-called GADM (GAD moment) was $7.66 \times 10^{22}\ Am^2$. The equatorial component of the dipole moment at 2000 had strength $|\mathrm{m_e}| \equiv \sqrt{(\mathrm{m_x^2} + \mathrm{m_y^2})} = 1.41 \times 10^{22}\ Am^2$ and was oriented along longitude $\phi_e = tan^{-1}(m_y/m_x) = 108.4E$. The south geomagnetic pole is the projection of the geocentric dipole moment vector onto the Earth's surface, and the north geomagnetic pole (NGP) is its antipode. The (geocentric) colatitude and east longitude of the NGP are given by:

$$\begin{aligned} \theta_N &= cos^{-1}\left(-\frac{g_1^0}{g}\right) = cos^{-1}\left(-\frac{m_z}{|\mathbf{m}|}\right); \\ \phi_N &= tan^{-1}\left(\frac{h_1^1}{g_1^1}\right) = tan^{-1}\left(\frac{m_y}{m_x}\right) \end{aligned} \tag{3}$$

where $g = \sqrt{(g_1^1)^2 + (h_1^1)^2 + (g_1^0)^2}$. In 2000 the NGP was located at (79.6N, 71.6W). Note that the geomagnetic poles defined this way are distinct from the magnetic poles (or dip poles), the locations on Earth's surface where the field orientation is vertical. The distinction is due to the fact that the dip pole locations are affected by the nondipole part of the field and the dipole part.

There are multiple reasons why the geomagnetic dipole moment and its secular change are important properties of

the geodynamo. The main observational reason has already been discussed: The core field at the Earth's surface is predominantly dipolar. The dipolar field far exceeds the nondipole field, especially in time average where the axial dipole dominates. Other reasons for considering the dipole moment as a distinct entity concern its role in the geodynamo. The geomagnetic dipole moment is a weighted integral of the transverse electric currents in the core (see Eq. 6). It is therefore an intrinsic, frame-invariant, and global property of the Earth (other moments of the field have some of these attributes but they are smaller and less persistent). Furthermore, the dipole moment can be determined using surface measurements alone according to Eq. 2. It differs in this regard from other global measures of geodynamo activity such as magnetic and kinetic energies, heat flow, and Ohmic dissipation, which cannot be determined directly from surface observations.

History of the dipole moment

Dipole axis motion

Because magnetic orientation was the primary method of navigation during the age of exploration, there is a globally distributed record of magnetic directional data that provides a picture of the dipole moment direction and its secular change starting around 1,600 AD (Jonkers et al. 2003). As Fig. 2 shows, both the latitude and the longitude of the NGP have changed in historical times. Between 1650 and 1860 the tilt angle increased from about 7.5° to 11.4°, while the NGP drifted generally westward through about 30° of longitude (Fraser-Smith 1987; Bloxham and Jackson 1992; Jackson et al. 2000). Since then, the westward motion of the pole has continued, while its north–south motion has reversed. From 1860 to 1960, the tilt remained almost constant. Then starting about 1970 the pole began to move northward, and by 2000 the tilt had decreased by more than 1°. This poleward motion of the dipole moment vector is evidently continuing. According to the model POMME 2.5 (Potsdam Magnetic Model of the Earth) derived from Ørsted and CHAMP (Challenging Minisatellite Payload) satellites (Maus et al. 2004), the NGP moved further northward by 0.1° between 2000 and 2002.5, and has moved an additional 0.1° northward since 2002.5 according to the 2005 International Geomagnetic Reference Field (IGRF, http://www.ngdc.noaa.gov/seg/geomag/models.shtml).

The sustained westward motion of the NGP evident in Fig. 2 corresponds to an average angular velocity of the dipole moment relative to the crust of −0.05 to −0.1° longitude per year, a motion that used to be interpreted as evidence for a retrograde differential rotation of the outer core relative to the mantle and crust (Bullard et al. 1950; Yukutake 1967). This explanation is no longer favored, however, because archeomagnetic and paleomagnetic data now indicate that the dipole axis motion over longer time intervals is highly irregular and includes abrupt directional changes.

Over the past several thousand years the NGP has traced out an irregular sequence of prograde and retrograde loops, generally within 15° of the geographic pole (Ohno and Hamano 1992; Constable et al. 2000; Johnson et al. 2003). The path of the NGP over the last 2 *kyr* determined from archeomagnetic pole measurements (Merrill et al. 1998) and from the CALS7K.2 archeomagnetic field model (Korte and Constable 2005) are shown in Fig. 2b. The underlying cause of this irregular motion is not yet established, but its kinematic effect is clear: It suppresses the equatorial component of the geomagnetic dipole, leaving only the axial part, the GAD, in time average. The length of time needed for this averaging out process is longer than it would have been if the NGP only moved westward, but is still rather short on the order of a few thousand years (Constable and Parker 1988; Carlut et al. 2000).

Recent decrease in dipole strength

Direct measurements of the dipole moment, beginning with Gauss' famous 1839 analysis (Leaton and Malin 1967; Malin 1982) and continuing into the era of magnetic satellites (Langel et al. 1980; Olsen et al. 2000), reveal a sustained decrease in moment strength. As shown in Fig. 2a, the strength of the dipole moment has decreased from $|\mathbf{m}| = 8.5 \times 10^{22}\ Am^2$ in 1840 to $7.79 \times 10^{22}\ Am^2$ in 2000. The average rate of decrease over the intervening 160 years was $|\dot{\mathbf{m}}| \simeq 1.40 \times 10^{12}\ Am^2 s^{-1}$, an overall rate of nearly 6% per century. The average decrease in the strength of the axial dipole moment (ADM) over the same 160 years was $|\dot{m}_z| \simeq 1.33 \times 10^{12}\ Am^2 s^{-1}$, accounting for about 95% of the total moment drop during that period. The latest satellite and observatory magnetic measurements confirm this trend. According to the POMME 2.5 satellite model (Maus et al. 2004) the dipole moment strength decreased by an additional 0.146% between epochs 2000 and 2002.5, very nearly equal to the historical 6% per century rate. By 2005 the strengths of the dipole moment and its axial component had fallen to $|\mathbf{m}| = 7.77 \times 10^{22}$ and $|m_z| = 7.644 \times 10^{22}$, respectively, according to the 2005 IGRF. As many authors have noted, if the present-day decrease were to continue at the same (linear) rate, the dipole moment would be reduced to zero within 2000 years (Leaton and Malin 1967; McDonald and Gunst 1968; Fraser-Smith 1987; Olson 2002). However, the nearly uniform rate of decrease since 1840 may not apply further into the past. Archeomagnetic measurements indicate a somewhat slower decay rate (see below) and Gubbins et al.

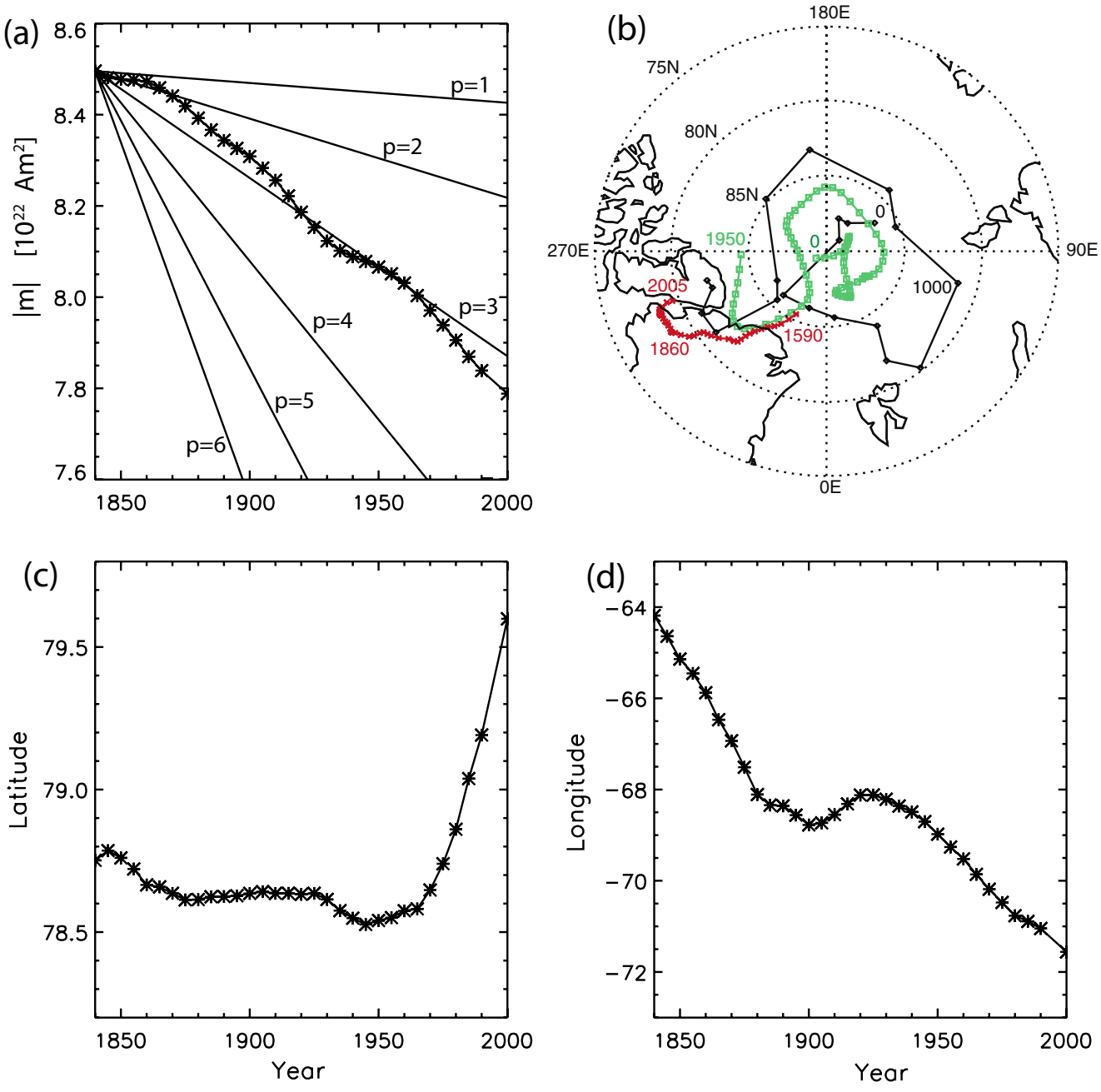

Fig. 2 Recent evolution of the geomagnetic dipole moment. **a** Change in dipole moment strength from 1840 to 2000 (*symbols*) compared with theoretical free decay rates of fundamental ($p = 1$) and higher mode ($p > 1$) dipole fields in the core, calculated using Eq. 4, assuming an electrical conductivity of $\sigma = 4 \times 10^5\ Sm^{-1}$. **b** NGP for the past 2,000 years. *Crosses*: pole since 1590 in 10-year intervals from historical field model gufm1 (Jackson et al. 2000), Ørsted satellite field model (Olsen et al. 2000), and 2005 IGRF field model. *Squares*: NGP 0–1950 at 25-year intervals from core field model CALS7K.2 by Korte and Constable (2005). *Diamonds*: mean archeomagnetic poles 0–1900 from Merrill et al. (1998). **c**, **d** NGP latitude and longitude, 1840–2000

(2006) have proposed that the present episode of rapid decrease actually commenced around 1840.

The equatorial moment strength has also decreased since 1840 at an average rate of $|\dot{m}_e| \simeq 5 \times 10^{11}\ Am^2 s^{-1}$, which is nearly 11% per century. In percentage terms this is even faster than the axial component decrease and accounts for the poleward motion of the NGP since 1970 as shown in Fig. 2b,c. In absolute terms, however, the decrease of the axial moment is the most important change in the present-day dipole as well as the most important change in the past couple of thousand years and is the main subject of our analysis.

We can put the present-day dipole moment strength decrease into physical perspective by comparing it with the theoretical Ohmic-free decay rate of dipole fields in the core. In Ohmic-free decay (the decay due to electrical resistance alone, without any effects of fluid motion) the dipole moment in a sphere with radius r_c and uniform electrical conductivity σ decays according to:

$$\mathbf{m} = \sum_{p=1}^{\infty} \mathbf{m}_p \, exp(-t/\tau_p) \tag{4}$$

where p is the radial mode number, $\mathbf{m}_p$ is its amplitude at time $t = 0$, and $\tau_p = \mu_0 \sigma r_c^2/(p\pi)^2$ (Moffatt 1978). Figure 1 shows the magnetic field lines and the electric current density of a fundamental ($p = 1$) mode dipole field, which has the slowest free decay rate of any magnetic field mode in the core. Using $r_c = 3480$ km for the core radius and $\sigma = 4 \times 10^5$ Sm^{-1} (corresponding to a magnetic diffusivity of $\lambda = 1/\mu_0\sigma = 2$ $m^2 s^{-1}$) for the electrical conductivity of the core (Poirier 1994, 2000) gives $\tau_1 = 19,580$ years for the free decay time of the fundamental mode and $\tau_p = 19,580/p^2$ for the free decay time of the pth dipole mode.

Initial free decay curves from Eq. 4 are shown in Fig. 2a in comparison with the observed changes in geomagnetic dipole moment strength. The time constant of the observed moment change over the past 160 years is about $\tau = |\mathbf{m}|/|\dot{\mathbf{m}}| \simeq 1840$ years. For an assumed electrical conductivity in the core 4×10^5 Sm^{-1}, this exceeds the fundamental dipole mode decay rate by a factor $\tau_1/\tau \simeq 11$. The disparity is even greater if a higher electrical conductivity of the core is assumed. According to Secco and Schloessin (1989), $\sigma = 6 \times 10^5$ Sm^{-1} in the core, which implies $\tau_1/\tau \simeq 16$. It is clear that the present-day decrease is not free decay of the fundamental mode dipole field in the core.

Alternatively, can the present decrease represent an episode of free decay of a higher mode dipole field in the core? As indicated in Fig. 2a, the present-day decrease approximates the free decay rate of dipole modes $p = 3$ or 4, depending on the electrical conductivity assumed for the core. Higher mode dipole fields imply a layered structure of electric current beneath the core–mantle boundary with layer thicknesses roughly $(r_c - r_i)/p$. For $p = 4$ the electric current layer in the outer core would be about 600-km-thick. While it is theoretically possible that the present decrease is entirely due to free decay of such a uniform current sheet, it is unlikely the correct explanation for several reasons. First, the moment decrease has generally accelerated with time over the last 2,000 years according to the data in Fig. 3a. This behavior is inconsistent with free decay of a mixed-mode field in which the fast decaying, higher modes would disappear first, leaving the slowly decaying fundamental mode to dominate the dipole field at later times. Second, if free decay was the only mechanism

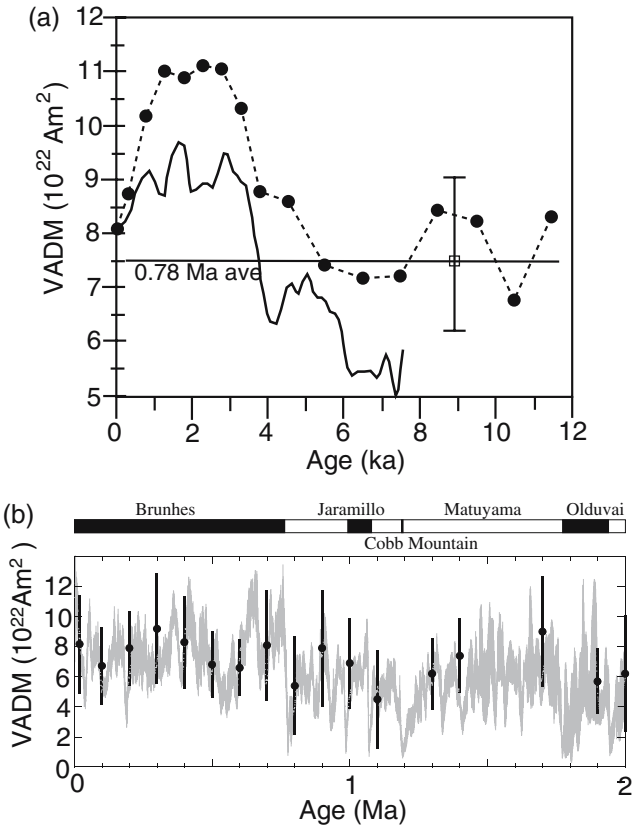

Fig. 3 **a** VADM over the past 12 ka (*symbols*) from combined archeomagnetic and paleomagnetic field intensity measurements by McElhinny and Senanayake (1982), Thouveny et al. (1993), and Yang et al. (2000) compared with the core field model CALS7K.2 (*solid curve*) by Korte and Constable (2005). Each *symbol* represents an average over several centuries. **b** VADM over the past 2 Ma from a stack of paleointensity curves obtained from sediment cores by Valet et al. (2005). *Top bar graph* shows major polarity chrons; *symbols* with error *bars* are data from volcanic rocks used for moment calibration. The average and standard deviation for the current Brunhes chron is shown in subpanel **a**

at work, the energy in degrees $l \geq 2$ of the core field would also be decreasing. However, this does not appear to be the case. Analyses of the energy of the core field indicate that it has changed relatively little over this time period (Verosub and Cox 1971; Benton and Voorhies 1987; DeSantis et al. 2003), despite the fact that increasing resolution of the core field introduces a bias into magnetic energy estimates. Finally, we demonstrate in the next section that the sources of dipole moment change on the core–mantle boundary are very heterogeneous, quite unlike a free decay process. We therefore conclude that the geodynamo has not simply shut itself off. Dynamical processes must be at work in the core, extracting energy from the dipole field and causing the moment to decrease faster than it would by free decay alone.

What other mechanisms are available to change the dipole moment? Fluid motion, which we have ignored so far in this discussion, can act to increase and diminish the dipole moment. As it is now understood, the geomagnetic dipole moment is generated mostly by convection in the outer core through an induction process related to the α-dynamo mechanism (Busse 2000; Roberts and Glatzmaier 2000; Davidson 2001). Because it is affected by the Coriolis acceleration due to the Earth's rotation, convection in the outer core has a property called *helicity* in which the vorticity and velocity of the fluid motion are correlated. Through its helicity, the convective motions transform toroidal-type magnetic field (toroidal magnetic field lines are wound in the core like a ball of string) into poloidal-type magnetic field (poloidal magnetic field lines have a radial component and extend beyond the core, the dipole field being an example). Helical induction transfers magnetic energy from the toroidal field into poloidal field, first on the length scales of the convective motion, and then to larger length scales, such as the dipole field. According to numerical models of the geodynamo, the convective helicity is negative on average in the northern hemisphere and positive on average in the southern hemisphere of the core (Olson et al. 1999; Christensen et al. 1999; Glatzmaier 2002; Takahashi et al. 2005); and this is the primary reason why the core field tends toward a time-averaged GAD configuration. The efficiency of this helical induction process governs the rate of energy flow into the dipole field, and according to these same numerical dynamo models, controls the strength of the time-averaged dipole moment.

Fluid motion in the core can also act to reduce the dipole moment strength by transferring energy from the dipole to other harmonics of the magnetic field as in ordinary turbulent cascade processes. Transfer of energy from the dipole by fluid motion can and likely does occur at times throughout the whole outer core. An example where this process can be inferred from geomagnetic secular variation is the reduction of the dipole moment through redistribution of magnetic flux over the core–mantle boundary by the flow in the outer core. For the ADM, this particular process occurs by meridional advection of magnetic flux, as we demonstrate in a later section. Fluid motion within the core can also promote the reduction of the dipole moment by enhancing magnetic diffusion. Here, the fluid motion sharpens the gradients in the magnetic field within the core leading to shorter characteristic length scales, accelerated magnetic diffusion, and increased magnetic field line reconnection (Moffatt 1978). These moment reduction mechanisms must be subordinate, on average, to moment-enhancing mechanisms such as the one described in the preceding paragraph, for otherwise the geodynamo would not be self-sustaining. However, it is possible for the reduction mechanisms to exceed the growth mechanisms for some time, causing a transient decrease in the dipole moment and even a polarity change.

Is there evidence that these types of dynamical moment-reducing processes are active in the geodynamo today? Because the dipole tilt is currently decreasing, we can conclude that the energy now being lost from the axial dipole is not being transferred into the equatorial dipole. We have already mentioned in connection with the GAD reference state that the nondipole terms in the core field fluctuate with century time constants. Because the time constants for all nondipole field components are shorter than the time constant of dipole moment decrease, the energy in the dipole is not being transferred into any single nondipole field component (the quadrupole field is now growing, but not fast enough to account for all of the dipole decrease). Instead, it *appears* that the energy in the dipole field is being redistributed among the higher harmonics of the field, a process that is opposite to the dominant energy flow that is thought to sustain the dipole in a long time average. In a later section we analyze the field and its secular change on the core–mantle boundary. We show evidence that the moment-reducing mechanisms of advection and diffusion are indeed active today, each contributing to the observed moment decrease.

The archeomagnetic dipole moment

Before examining how fluid advection and diffusion of magnetic field in the core combine to produce rapid dipole moment decrease, it is important to establish how long the present episode of decrease has been in place and to compare this event with the behavior of the dipole moment at earlier times. The plots in Fig. 3 show the virtual axial dipole moment (VADM) over time. The VADM is determined from the intensity of magnetization of crustal rocks or archeological artifacts, and assumes the inducing field is GAD (Merrill et al. 1998). The data in Fig. 3a represent time averages of historical measurements plus measurements from rock magnetization at archeological and recently active volcanic sites over the past 12,000 years (McElhinny and Senanayake 1982; Thouveny et al. 1993; Yang et al. 2000). Following usual procedures, the VADM data was time-averaged in bins to reduce contamination by the nondipole part of the field. Figure 3a also shows dipole moment variations over the past 7,500 years from the CALS7K.2 core field model of Korte and Constable (2005) and the mean and standard deviation of the intensity for the whole of the current Brunhes normal polarity chron as determined by Valet et al. (2005).

The current episode of dipole moment decrease evidently commenced between 1000 and 2000 BP, following an approximately 2,000 year-long interval when the average

strength was high, nearly 11×10^{22} Am^2 according to the archeomagnetic VADM, and nearly 9.5×10^{22} Am^2 according to the CALS7K.2 field model. The moment decrease has generally accelerated over the past millennium. This most recent maximum ended around 3500 BP and was preceded by a longer period of intensity increase that commenced around 6000 BP, which in turn followed a shorter period of moment decrease starting around 9000 BP.

Two additional points concerning Fig. 3a are worth emphasizing here. First, although the intensity drop in the past few hundred years might appear to be more rapid than the characteristic rates of change for the time interval as a whole, this may be a sampling bias. Higher resolution archeomagnetic measurements (Yang et al. 2000) indicate that additional shorter period intensity fluctuations are also present during this period, but these were eliminated by the binned averages in Fig. 3a to emphasize the major trends. Furthermore, the root-mean-square variation of the moment strength over the past few hundred years in the CALS7K.2 field model is not anomalous compared to its value over the whole 7,500-year period (Constable and Korte 2005). Another significant point is that the present-day moment is about equal to the average for the entire 0.78 Ma Brunhes polarity chron, while the peak moment near 2000 BP is close to the maximum for the entire Brunhes chron (Valet et al. 2005). In short, the present-day moment is above its long time-averaged strength, as indicated in the data in Table 1. Although it is decreasing rapidly, the dipole moment is still large in absolute terms. All of this is evidence against the interpretation that the present-day decrease signals the disappearance of the dipole, or that a polarity reversal is imminent.

The paleomagnetic dipole moment

Paleomagnetic intensity measurements on rocks of various ages reveal dipole moment fluctuations over a wide spectrum of frequencies, corresponding to periodicities from less than one thousand years to hundreds of millions of years (Constable and Johnson 2005). Inferring the intensity of the ancient paleomagnetic field from the intensity of magnetized volcanic and sedimentary rocks is a challenging task. For comprehensive reviews of the various paleointensity measurement techniques and their results, see Selkin and Tauxe (2000), Valet (2003), and Yamamoto and Tsunakawa (2005). Very briefly, volcanic rocks can provide absolute vector data and generally yield the best intensity values, but these are typically discrete in time. More continuous records of the dipole moment come from the magnetization of marine and terrestrial sediments, but the conversion from the measured sample magnetization to the intensity of the inducing field is often problematic.

Table 1 Average dipole moment over different time intervals

Time interval	Average dipole moment	Reference
160 a	8.12×10^{22} Am^2	Jackson et al. (2000)
7 ka	6	Korte and Constable (2005)
10 ka	8.75 ± 1.6	Valet et al. (2005)
15–50 ka	4.5	Merrill et al. (1998)
300 ka	8.4 ± 3.1	Selkin and Tauxe (2000)
800 ka	7.5 ± 1.5	Valet et al. (2005)
0.8–1.2 Ma	5.3 ± 1.5	Valet et al. (2005)
0.3–5 Ma	5.5 ± 2.4	Juarez and Tauxe (2000)
0.5–4.6 Ma	3.6 ± 2	Yamamoto and Tsunakawa (2005)
5 Ma	7.4 ± 4.3	Kono and Tanaka (1995)
0.3–300 Ma	4.6 ± 3.2	Selkin and Tauxe (2000)

Moment oscillations

Paleomagnetic vector data older than about 50 ka is relatively sparse, which limits our ability to track absolute dipole moment variations much further back in time than the archeomagnetic window. But recently, several long time series of paleointensity were constructed by stacking sediment records and calibrating the resulting composite curves against volcanic intensity data for periods up to 2 Ma (Guyodo and Valet 1999; Gee et al. 2000; Yokoyama and Yamazaki 2000; Valet et al. 2005). A 2-Ma composite of VADM records from marine sediments by Valet et al. (2005) is shown in Fig. 3b. This and other similarly constructed composite records generally show a series of large amplitude oscillations about a mean moment strength with characteristic periods in the 10–80 ka range and peak-to-trough moment variations as large as a factor of four or five.

The cause of these oscillations is unknown. Occasionally, long period fluctuations are seen in these records that may have an origin in climate variations. For example, Yokoyama and Yamazaki (2000) report 100-ka intensity variations, suggestive of the period of orbital eccentricity variations. But for the most part, the fluctuations in these records occur over a wide frequency band, rather than discrete frequencies. As pointed out by Valet et al. (2005) and others, several lines of evidence point to a geodynamo origin for these oscillations. First, the mean VADM in Fig. 3b during the current Brunhes polarity epoch differs from earlier epoch means. Second, the polarity reversals occur during VADM lows, a relationship that was seen in other paleomagnetic reversal records (Merrill and McFadden 1999).

The dipole moment through geologic time

Because continuous magnetic intensity records are lacking for older times, the usual way of characterizing dipole

moment variations deep into the geologic past is to compare means and standard deviations of moments averaged over different time intervals (Merrill et al. 1998). Even though the amount and quality of paleointensity data is growing rapidly, we do not yet have a clear picture of the dipole moment through Earth's history. For example, although we know the geomagnetic field has existed for 3.5 Ga or longer, we only have a crude estimate of the average moment over that time. In addition, while there is plenty of evidence for dipole strength variations on geologic time scales, there is no clear evidence for a secular trend and little agreement on the time and amplitude of long-term moment fluctuations. With these uncertainties in mind, we summarize in Table 1 some recent estimates of means and standard deviations of the paleomagnetic dipole moment strength over different time intervals.

Over the past 10 ka, the archeomagnetic intensity data in Fig. 3a give $|\mathbf{m}| = 8.75 \pm 1.6 \times 10^{22}\ Am^2$, whereas the more detailed archeomagnetic field model by Korte and Constable (2005) that takes the nondipole field into account when calculating the dipole moment results in a smaller value, around $|\mathbf{m}| = 6 \times 10^{22}\ Am^2$ for the past 7 ka. Before this, between 15 and 50 ka, archeomagnetic intensity data indicates the moment was significantly smaller, around $|\mathbf{m}| = 4.5 \times 10^{22}\ Am^2$ (Merrill et al. 1998).

Average moments were estimated for a few individual polarity chrons. For the current Brunhes chron, the sedimentary records shown in Fig. 3b give $|\mathbf{m}| = 7.5 \pm 1.5 \times 10^{22}\ Am^2$, whereas the same records give $|\mathbf{m}| = 5.3 \pm 1.5 \times 10^{22}\ Am^2$ during the preceding 400 ka (Valet et al. 2005). The large average moment during the Brunhes chron was substantiated by several other studies (Guyodo and Valet 1999; Gee et al. 2000). In particular, the study by Selkin and Tauxe (2000) gave $|\mathbf{m}| = 8.4 \pm 3.1 \times 10^{22}\ Am^2$ for the past 300 ka, generally consistent with the results in Fig. 3b.

The first estimates of the average dipole moment for the past 5 Ma gave values close to the present-day strength. For example, Kono and Tanaka (1995) found $|\mathbf{m}| = 7.4 \pm 4.3 \times 10^{22}\ Am^2$. However, more recent estimates are significantly lower than this. Juarez and Tauxe (2000) found $|\mathbf{m}| = 5.5 \pm 2.4 \times 10^{22}\ Am^2$ for 0.3–5 Ma, and Yamamoto and Tsunakawa (2005) report $|\mathbf{m}| = 3.6 \pm 2 \times 10^{22}\ Am^2$ for 0.5–4.6 Ma. Clearly, the trend is toward lower moment estimates for this time period.

Determining the average moment on geologic time scales becomes increasingly difficult with age due to loss and overprint of rock magnetic information. A survey by Kono and Tanaka (1995) of intensity measurements on rocks between 100 and 3,500 Ma shows evidence for moment strength fluctuations on roughly 1,000 Ma time scales, but little or no evidence of a secular trend. Overall, their study found dipole moments generally lower than, but within a factor of 2, its present-day value for most of that time. A more recent study by Selkin and Tauxe (2000) gives $|\mathbf{m}| = 4.6 \pm 3.2 \times 10^{22}\ Am^2$ for 0.3–300 Ma, again with no secular trend apparent. Similar results were found by Juarez et al. (1998) for 0–160 Ma.

The large standard deviations associated with these estimates indicate there may be long period fluctuations in dipole moment strength that correlate with indicators of variability in the mantle, such as changes in tectonic plate motions or the activity of volcanic hotspots, or with other indicators of variability in the core. Heller et al. (2003) find evidence for a bimodal distribution of intensities in the past 230 Ma, perhaps related to plate tectonic or other mantle processes. Hale (1987) and Biggin and Thomas (2003) have interpreted dipole moment changes and other paleomagnetic data in terms of major events in the Earth's history, including plate tectonics and the nucleation of the inner core. Another indication of long-term change in the geodynamo is the secular change in polarity reversal frequency, which is discussed in more detail in the next section. The dipole moment during the Cretaceous polarity superchron (82–125 Ma) is of particular interest in this context because some paleomagnetic data (Valet et al. 2005) and some geodynamo models (Larson and Olson 1991) predict that polarity chron length should correlate with dipole moment strength. A number of studies were made of the paleomagnetic intensity at different parts of the superchron, but unfortunately, these give rather different results, with some indicating average or weak moment (Zhu et al. 2001; Pan et al. 2004), while others indicating anomalously strong moment (Tarduno et al. 2001).

In summary, the dipole moment fluctuates on time scales ranging from centuries to tens of thousands of years and perhaps longer. The amplitudes of these fluctuations are variable, but are generally limited to 50–75% of the mean value. There is growing evidence that today's dipole moment and the average dipole moment during the present polarity chron are substantially stronger than the longer term average. As the data in Table 1 indicates, we have yet to determine the average dipole moment over geologic time with adequate precision. Even when the stronger moment during the recent past and possible long-term fluctuations are taken into account, there is little evidence for a secular trend in dipole moment over the Earth's history.

Polarity reversals

A major achievement of paleomagnetism is the delineation of the polarity reversal record over the past 160 Ma. For the purposes of this review, we use the Merrill et al. (1998) definition of polarity reversals, transitions between two quasiequilibrium geomagnetic states that have statistically similar characteristics, apart from the change in sign of the

dipole moment. The paleomagnetic record of reversals is quite extensive, and much of it is beyond the scope of this review. The reader is referred to Jacobs (1984), Merrill and McFadden (1999), and Constable (2003) and references therein for recent summaries of the reversal record and its geological and geophysical implications.

As is the case with dipole moment variations, many important aspects of polarity reversals are poorly understood. For example, the morphology of the transition field is not yet agreed upon. There are two basic end-member models, the first consisting of dipole moment rotation from one hemisphere to the other, the second consisting of loss of the ADM followed by regeneration with the opposite polarity. Each of these appears too simple to explain all transition field data, which are complex and evidently vary from one reversal to another (Constable 2003). Another unresolved issue is the significance of individual reversals. Unlike the periodic reversals of the solar dynamo, geomagnetic reversals are aperiodic and appear to be largely independent events (Merrill and McFadden 1999) with an average frequency of one in about 240,000 years over the past 5 Ma (Constable 2003). The aperiodic character of individual reversals is exemplified by the fact that the last reversal occurred 785,000 years ago, so the present-day Brunhes chron is almost three times longer than the average polarity chron in the recent geologic past.

It is known that polarity reversals do not require an external perturbation to occur. Many numerical dynamo models exhibit polarity reversals, both quasiperiodic (Wicht and Olson 2004; Takahashi et al. 2005) and aperiodic (Glatzmaier et al. 1999; Kutzner and Christensen 2002) in time. These model reversals are internally excited instabilities in the flow or the magnetic field, or both. In general, polarity reversals in dynamo models tend to occur when the dipole moment is weak and its tilt is large and variable. This is consistent with the known behavior of paleomagnetic reversals as discussed below. Quasiperiodic reversals in numerical dynamo models indicate oscillatory dynamo action. Here, the dipole field oscillates out of phase with the toroidal field, the part of the magnetic field in the core that has no radial component. Aperiodic reversals in numerical dynamo models usually begin with a fluctuation in the fluid motion, which in turn precipitates a magnetic instability, which sometimes leads to polarity change, particularly when the dipole moment is low (Glatzmaier and Roberts 1995; Kutzner and Christensen 2002). The irregular time intervals between reversals in this type of dynamo are a consequence of the chaos in the fluid motion. If this is the mechanism by which reversals occur in the core, then individual geomagnetic polarity reversals may have little significance of their own.

Although individual geomagnetic reversals appear to be independent events, the average rate of reversals has changed systematically with time, and this may have broad geophysical significance. In particular, the average frequency of polarity reversals has steadily increased since the Cretaceous superchron, a 43-Ma interval ending around 82 Ma that was devoid of polarity changes (Merrill and McFadden 1999; Constable 2003). This long time scale increase in reversal frequency is suggestive of mantle control, partly because it correlates with changes in tectonic plate motions and volcanic hotspot activity (Courtillot and Besse 1987; Larson and Olson 1991), and partly because a 100-Ma time-scale fluctuation seems excessively long to have its origin in the core's own dynamics, independent of the mantle. Slow changes in the pattern and magnitude of heat flow or topography on the core–mantle boundary, in response to changes in the pattern of mantle convection or the distribution of mantle plumes, were implicated in this process (Courtillot and Besse 1987; Loper and McCartney 1986; Larson and Olson 1991; Olson 2003), but a full understanding of the connection between mantle dynamics and polarity reversal frequency remains elusive.

Despite the uncertainties surrounding the polarity reversal phenomenon, there are some characteristics that are well established and involve significant dipole moment changes. First, most reversals are associated with a large drop in the dipole moment that typically occurs before the major directional changes of the field. During many reversals the field intensity drops to about 25% of its normal value at the height of the directional transition (Lin et al. 1994; Tanaka et al. 1995; McFadden and Merrill 1997). Second, the duration of this intensity drop generally lasts 5,000 to 20,000 years (Merrill and McFadden 1999; Valet 2003), while the directional transition is usually shorter, typically lasting 2,000–7,000 years (Bogue and Paul 1993; Dormy et al. 2000; Clement 2004). We note that the rate of paleointensity decrease before polarity reversals is comparable to the present-day moment decrease rate.

The geomagnetic field on the core mantle boundary

The geodynamo is a fully three-dimensional process involving the whole of the core, and imaging the geodynamo from the surface is a major Earth Science objective. It is perhaps unfortunate that the geophysical methods, which have provided spectacular images of crust and mantle structure—seismic waves, gravity, and magneto-tellurics—do not provide a clear image of the geodynamo. The limitations of these methods in this context stem from the physical properties of the molten iron compounds in the outer core, particularly their low viscosity. The viscosity of liquid iron alloys is so low, even at elevated pressure (the kinematic viscosity of liquid iron measured at several kilobar pressure is around $10^{-4}\ m^2 s^{-1}$

De Wijs 1998; Dobson et al. 2000), that the outer core fluid cannot dynamically maintain large lateral heterogeneity of any property that is linked to its density. Because seismic wave speeds, electrical conductivity, and other properties of iron compounds that can be inferred from geophysical observations tend to have some relationship to density (Poirier 1994), there is no observable lateral variation expected for these properties in the outer core (Stevenson 1987).

The clearest image of the structure of the geodynamo available to us comes from the pattern of the core field and its secular variation on the core–mantle boundary. Much information about the geodynamo was gleaned by interpreting the geomagnetic field on the core–mantle boundary in terms of the flow at the top of the outer core (Gire et al. 1986; Voorhies 1986; Jault et al. 1988; Bloxham 1989; Gire and LeMouël 1990; Bloxham and Jackson 1991; Jackson et al. 1993; Jackson 1997; Pais and Hulot 2000; Holme and Whaler 2001; Hulot et al. 2002; Amit and Olson 2006). Here we summarize what was learned from the core field and its secular variation as it applies to dipole moment change. For this purpose we use the time-dependent geomagnetic field model gufm1 of Jackson et al. (2000) for years 1840–1990, which was derived from ground-based magnetic observatory and navigation records along with the 1980 Magsat satellite data. We also use the Øersted satellite field model (Olsen et al. 2000) for epoch 2000. Because of interference from crustal magnetization and other near-surface effects, these core field models use spectral regularizations that effectively remove structure above spherical harmonic degree $l_{max} \simeq 13$ (Bloxham et al. 1989; Bloxham and Jackson 1992; Langel and Hinze 1998), which limits the scale of magnetic and flow structures that can be imaged on the core–mantle boundary to about 500 km or larger.

Subpanels a and b of Fig. 4 are the maps of the radial component of the core field on the core–mantle boundary for the years 1900 and 2000, respectively. Figure 4c is a map of $B_r \cos\theta$ at epoch 1980 and Fig. 4d is the secular variation (time derivative) of this quantity at the same epoch. These maps reveal several important properties of the geodynamo. First, the field on the core–mantle boundary deviates substantially from a simple axial dipole, particularly in the 2000 map. The radial field is concentrated in several high-intensity patches or lobes, the most significant of these are located between 60 and 70° latitude in both hemispheres. Two large high-intensity patches appear in the northern hemisphere—one below North America, the other beneath Siberia. A somewhat similar pattern of normal polarity flux concentration is also present in the southern hemisphere, although it takes the form of a single large patch with two lobes, rather than distinct separate patches. Although they are not completely stationary, these high field intensity regions are persistent structures, clearly identifiable in field maps 100 years apart. In 1900 the North American patch is centered near 45°N latitude; the southern hemisphere lobes are more poleward of 70°S latitude at both epochs. In addition to strong normal polarity flux patches at high latitudes, the 2000 core field includes local intensity minima near both geographic poles where an axial dipole field would be strongest. Local intensity maxima also appear at low latitudes, particularly beneath equatorial Africa (Jackson 2003).

There are also several regions in each hemisphere where the radial field has the wrong polarity, the so-called reversed flux patches. The largest reversed flux patches are located in the southern hemisphere beneath the South Atlantic, but there are several in the northern hemisphere as well, including some in the polar regions and one beneath Bermuda. Comparison of the 1900 and 2000 maps shows that unlike the high-latitude normal polarity flux patches, some of these reversed flux patches have formed within the past century, and several have become stronger over this period time (Gubbins 1987).

Figure 4c,d shows how these normal and reversed flux concentrations on the core–mantle boundary contribute to the geomagnetic ADM and its rate of decrease. Figure 4c is a map of the axial component of the dipole moment $B_r \cos\theta$, the integrand of m_z in Eq. 2 on the core–mantle boundary. The most striking aspect of this map is the overwhelming contribution of the high-latitude normal polarity flux patches to the ADM. Essentially, these structures are the source of the axial geomagnetic dipole moment. Significant negative contributions to the axial dipole are confined to the region beneath the South Atlantic where the large reverse flux patches are located.

A related but somewhat more complex picture emerges from the pattern of ADM secular change shown in Fig. 4d. Positive on this map indicates regions where the ADM is being weakened, whereas negative indicates regions where it is being strengthened. Both types of regions are represented well on the core–mantle boundary at this epoch, and indeed at every epoch we have examined. This is yet another testimony to the highly dynamical environment of the core. Even when the dipole moment is rapidly diminishing, there are extensive regions in the core where the dipole moment is actively being regenerated with the decrease of the dipole moment being the small difference between these two types of regions. Note that the Atlantic hemisphere is more active in this process than the Pacific hemisphere.

Figure 4e,f shows the partial contributions to the ADM by hemisphere and by magnetic field polarity between 1840 and 1990. In these plots, it is the relative contributions from each hemisphere that have the most significance. The absolute values are more difficult to interpret because large amounts of flux cancellation occur within each hemisphere. Even so, these maps point to the localities on the core–

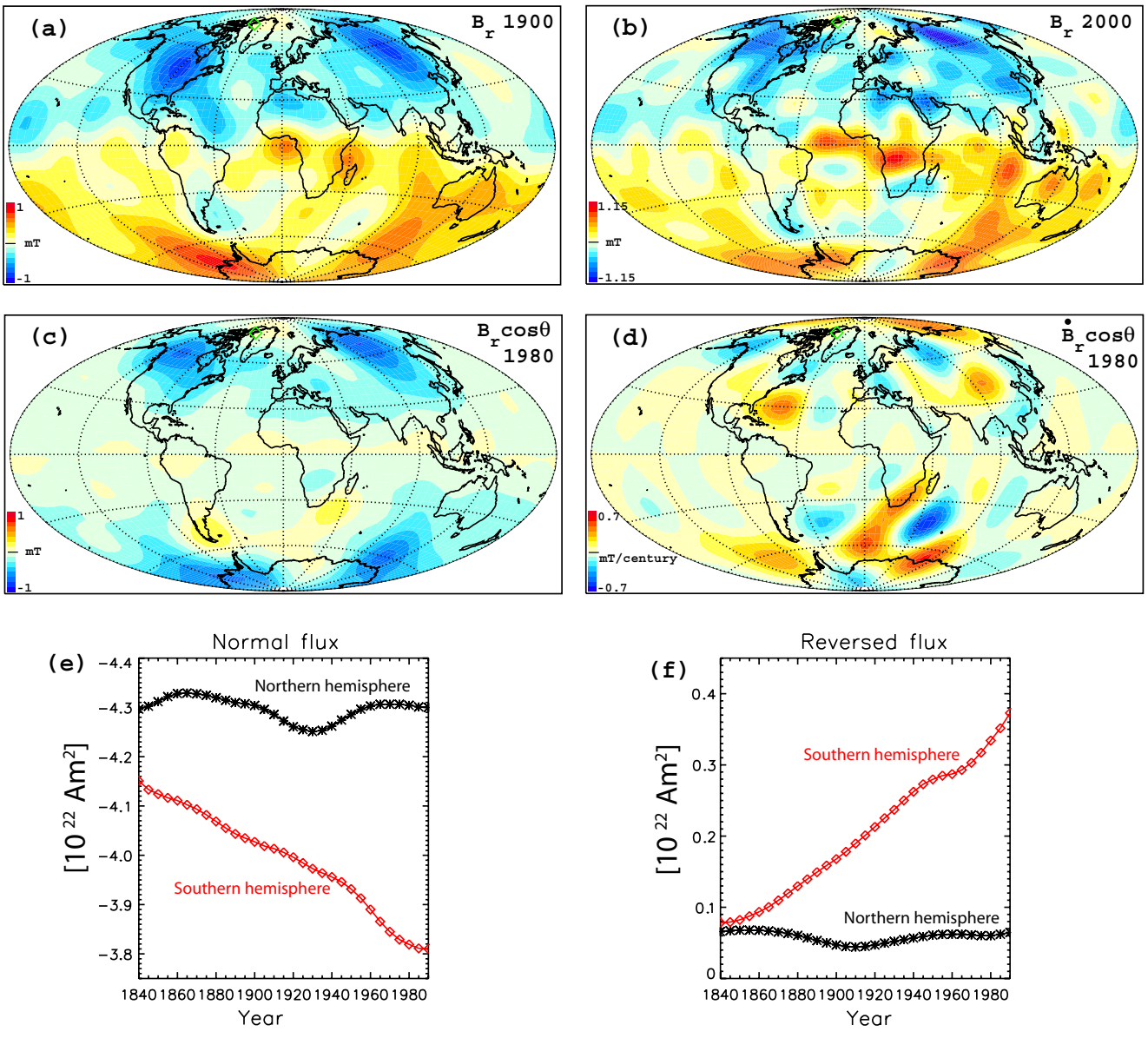

Fig. 4 The geomagnetic field and the geomagnetic ADM on the core–mantle boundary, 1840–2000. Maps **a**–**d** include continental outlines for reference. **a** Radial component of the core field B_r at 1900 (Jackson et al. 2000) with NGP (*open diamond*) shown for reference. **b** B_r at 2000 from Ørsted satellite field model (Olsen et al. 2000). **c** $B_r \cos\theta$ at 1980 showing the local contributions to the axial moment. **d** $\dot{B}_r \cos\theta$ at 1980 showing the local contributions to the rate of change in the axial moment. **e** Contribution to the axial moment from normal magnetic flux by hemisphere since 1840. **f** Contribution to the axial moment from reverse magnetic flux by hemisphere since 1840

mantle boundary where major GADM changes occur. Figure 4e,f reveals that the dipole moment decrease attributable to changes in the normal and reverse magnetic flux in the northern hemisphere of the core–mantle boundary are relatively small over this time interval. In contrast, although the southern hemisphere contributes less to the overall dipole moment, it contributes far more to its secular change. This demonstrates that the current decrease of the dipole moment is mostly a southern hemisphere phenomenon. As we show in a later section, the current dipole decrease involves a major persistent component of the circulation at the top of the outer core, the large anticyclonic gyre beneath the South Atlantic and Indian Oceans. This gyre advects normal polarity field toward the equator and reversed field toward the South Pole, reducing the dipole moment. In addition, the major reversed flux

patches in the southern hemisphere are located within or adjacent to this gyre, and their formation and growth may be related to this flow structure.

The South Atlantic Anomaly (SAA)

The region on the core–mantle boundary that includes the weakened and reverse flux at midlatitudes of the southern hemisphere, extending from beneath the Indian Ocean to South America, is the source of the magnetospheric SAA. At the Earth's surface and at satellite altitudes, the SAA region appears as a roughly elliptical area several thousand kilometers in diameter in which the magnetic field intensity is weaker than would be expected for a simple inclined geocentric dipole (Pinto et al. 1992; Badhwar 1997; Heirtzler 2002). The minimum intensity in the SAA today is found just off the coast of Brazil, and amounts to about a 35% reduction at low-orbiting satellite altitudes.

The significance of the SAA comes from the effect of the low-intensity field on the Van Allen radiation belts. The two Van Allen radiation belts are low-latitude, torus-shaped regions in the magnetosphere consisting of charged particles extracted from the solar wind (Hargreaves 1992). The Van Allen radiation belts contain magnetically trapped electrons with energies up to about 10 MeV, protons of up to several hundred mega-electron-volts, and some helium nuclei. The inner radiation belt extends to two Earth radii and contains both electrons and protons, while the outer belt extends to about ten Earth radii and contains mostly electrons. These belts are approximately aligned with the geomagnetic dipole moment axis and are inclined with respect to the rotation axis by approximately the same amount as the dipole tilt, which is 10–11° (Brasseur and Solomon 1984). Because of the nondipole structure of the core field, the radiation belts vary in altitude over various parts of the Earth. The inner belt extends down to 200–800 km altitude above South America and the western portion of the South Atlantic where the field intensity is low, creating the region of the SAA (Heirtzler 2002). The SAA also fluctuates in time. On short time scales, its fluctuations are in response to variations in solar activity and magnetospheric conditions (Badhwar 1997); on long time scales it changes in response to the secular changes in the core field.

Satellites and other spacecrafts passing through this SAA are bombarded by 10 MeV protons at rates as high as 3,000 cm^{-2} s^{-1} (Lean 2005). It is known that particles with energies greater than about 1 MeV pose a threat to spacecraft systems (Carlowicz and Lopez 2002). Such energetic particles can degrade electronics, optics, solar panels, and other critical systems by breaking chemical bonds and disrupting crystalline structure. It is also well documented that radiation damage on satellites passing through the SAA causes problems with the operation of on-board electronic systems and malfunction of spacecraft components (Golightly et al. 1994; Konradi et al. 1994; Deme et al. 1999; Buhler et al. 1996). For example, the Hubble Space Telescope passes through the SAA multiple times each day, and has spent nearly 15% of its time in this particular environment, likely shortening its operational life. In the future, spacecraft must be designed with additional hardening to withstand the radiation in this environment, at the cost of significant additional mass.

SAA radiation also poses a potential threat to personal and biological systems during low Earth orbit. As they pass through tissue, heavy particles deposit their energy by ionizing water and proteins, causing cellular damage, modifying DNA and RNA, and increasing susceptibility to cancers and immune system disorders (Durante 2002). Ionizing radiation can directly affect DNA, leading to single and double strand breaks. The cell's ability to repair DNA damage becomes impaired, leading to DNA deletions and other forms of mutations (McCormack et al. 1988). As in the case of electronic components, protecting humans from particles in the mega-electron-volt range requires additional mass added to the spacecraft for shielding.

Are there health issues posed by the SAA at lower altitudes? Energetic particle fluxes at low altitudes are low due to atmospheric absorbtion and scattering. However, there is some indication of an SAA effect in the 5- to 10-km altitude range of commercial jet travel. For example, radiation dose rates as high as 0.3 mrem/h were measured along Paris-Buenos Aires flight paths beneath the center of the SAA (Bottollier-Depois et al. 2000), somewhat higher than expected for normal airline travel (Gundestrup and Storm 1999). At this rate, several hundred hours of exposure at this level would be needed to reach the 1 mSv (millisievert) annual limit traditionally recommended as a safety maximum for exposure to ionizing radiation. However, the concept of a safety threshold for low-level ionizing radiation is coming under increasing scrutiny and doubt. The recent 2005 Biological Effects of Ionizing Radiation VII report to the US National Academy of Sciences supports the "linear-no-threshold" model in which radiation-induced cancer risk increases linearly at low doses without a threshold so that even the smallest dose has the potential to cause a small but nonzero increase in risk to humans (BEIR VII Phase 2 2005). With increasing amounts of space and high altitude travel, the effects of exposure to such small radiation doses will likely become a more significant issue in the near future.

Suppose that the current trends persist in the southern hemisphere of the core–mantle boundary, the dipole moment continues to fall and the SAA continues to develop. What might be some of the consequences?

Sustained loss of dipole moment at its current rate for several more centuries would be expected to have major effects on the external field, with reductions in the radius of the magnetosphere and ionosphere ring currents (Sisco and Chen 1975) and changes in size of the polar cap (Glassmeier et al. 2004), all of which could change Earth's sensitivity to space weather events. If the decrease would continue for another ten centuries or so, the internal field would begin to assume a configuration close to what is regarded as the conditions typical of the onset of polarity reversal. During an actual reversal where the dipole moment typically falls to about 25% of its nominal value and the transitional field likely includes several dip poles including some near the geographic equator, the effects of such reduction would be seen and felt globally. The reduction in the magnetopause radius described above would be at its height. Visual effects that would become apparent in the early stages of a polarity change might include changes in the aurora australis, the southern lights. Now seen mainly over the South Polar region, they would appear closer to the equator as the SAA grows. A strongly nondipolar transition field might conceivably affect migratory animals, which now rely on the geomagnetic field to navigate (Phillips 1996; Walker et al. 2002; Mouritsen et al. 2004). More significant effects might come from the higher levels of ionizing radiation expected to reach the lower atmosphere in the densely populated low-latitude regions. The loss of the magnetic field could lead to spike occurrences of cancer and other radiation-induced maladies. However, there is little evidence that magnetic field-induced biological perturbations have happened before. Although it has long been speculated that the signature of polarity reversals might be seen in the paleontological record of extinctions, there is no established correlation between extinction rates and polarity reversals (Raup 1985). Evidently, the effects of weak geomagnetic field on biodiversity are not strong, either because the increased radiation is not severe enough, because the environmental change is slow enough to permit organisms to adapt to it, or because the external field strengthens as the internal field weakens. For example, it was proposed that the solar wind can induce an external field through interaction with the ionosphere that would be strong enough to protect the surface from cosmic radiation during times when the internal field is weak (Birk et al. 2004).

Geomagnetic images of flow in the core

We now address the question of how the present-day dipole moment decrease is occurring by examining the interaction of magnetic field and fluid motion just below the core–mantle boundary. Maps of the fluid velocity below the core–mantle boundary were derived for different epochs by assuming the magnetic field in the core acts like a passive tracer, frozen into and moving with the outer core fluid, the so-called frozen-flux assumption (Gire et al. 1986; Voorhies 1986; Jault et al. 1988; Bloxham 1989; Gire and LeMouël 1990; Bloxham and Jackson 1991; Jackson et al. 1993; Jackson 1997; Pais and Hulot 2000; Holme and Whaler 2001; Hulot et al. 2002; Amit and Olson 2006). The theoretical basis for the frozen-flux method is the magnetic induction equation in its infinite magnetic Reynolds number limit where effects of magnetic diffusion are assumed to be negligible in comparison with the effects of advection by the flow. In this limit the secular variation of the magnetic field is balanced by advection, tilting, and stretching of magnetic field lines by the outer core fluid motion. The magnetic Reynolds number for the core is defined as UL/λ where U is the characteristic outer core fluid velocity, L is the length scale of the flow, and λ is the magnetic diffusivity of the outer core fluid. Estimates for the core give $Rm \sim 300 - 500$ (Gubbins 1982; Bloxham 1989; Bloxham and Jackson 1991; Olson et al. 2002; Amit and Olson 2004), certainly large compared to one, although finite.

Just below the core–mantle boundary, close enough to the solid mantle that the radial core fluid velocity is small compared to the tangential fluid velocity **u**, but below the viscous boundary layer, the radial component of the magnetic induction equation in the frozen flux limit takes the form (Roberts and Scott 1965):

$$\frac{\partial B_r}{\partial t} + \mathbf{u} \cdot \nabla \mathrm{B_r} + \mathrm{B_r} \nabla \cdot \mathbf{u} = \mathbf{0} \tag{5}$$

where B_r is the radial magnetic field, t is time, and **u** is the fluid velocity tangent to the spherical core–mantle boundary. The physical interpretation of this equation is either in terms of frozen magnetic flux attached to the fluid or B_r on the core–mantle boundary playing the role of passive tracer for the core flow with Eq. 5 being the column-density conservation equation for this tracer. The inversion procedures that are used to convert B_r and its time derivative on the core–mantle boundary into maps of **u** in the outer core consistent with Eq. 5, including the limitations of these methods, are discussed in Bloxham and Jackson (1991).

An example of one such core flow map is shown in Fig. 5a for epoch 1980. This particular frozen-flux core flow was obtained by inverting Eq. 5 for **u**, assuming a combination of tangentially geostrophic and helical motion (Amit and Olson 2006). We selected this particular year for display because the field model is heavily constrained by Magsat satellite data, it lies a decade away from the 1990 terminus of the gufm1 field model, and is characterized by a large instantaneous GADM change, about 2 TAm^2s^{-1}. Like other core flows derived using frozen-flux (Bloxham

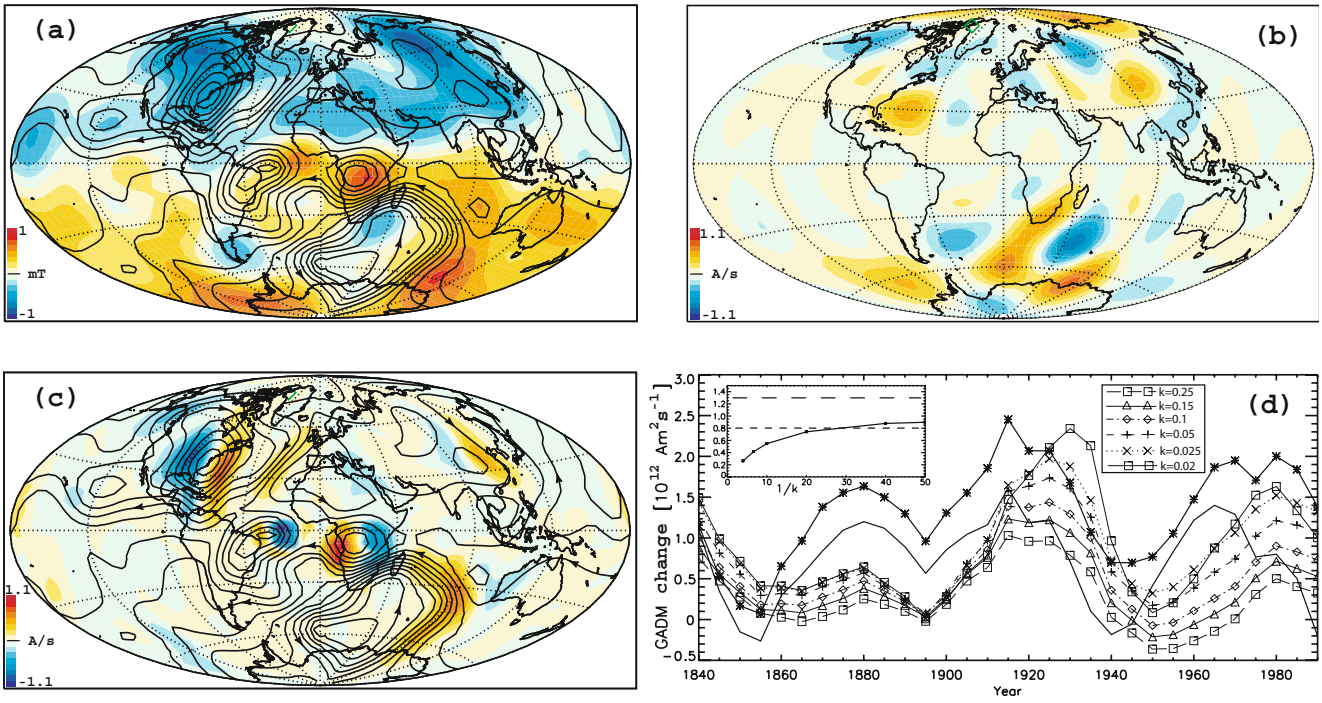

Fig. 5 Analysis of geomagnetic ADM change mechanisms on the core–mantle boundary. **a** Radial magnetic field B_r (*filled contours*) plus streamlines of frozen-flux core flow (*solid curves* with circulation direction *arrows*) at 1980. **b** ADM density change $\dot{\rho}_z$ defined in Eq. 9 at 1980. **c** Advective contributions to axial moment change from frozen-flux core flow (*filled contours*, in As^{-1}) with streamlines superimposed. **d** Contributions to axial moment change from frozen-flux core flow model for different model k values shown in *symbol key*, compared with the observed total axial moment change (*solid*, *asterisk*) and reduced axial moment change (*solid*) from 1840 to 1990, all in units of $10^{12}Am^2s^{-1}$. *Insert*: time-averaged frozen-flux advective moment change (*solid*, *asterisk*) vs model k value. Also shown are the observed time-averaged change (*long dash*) and the time-averaged reduced change (*short dash*)

1989, 1992; Jackson et al. 1993; Holme 1998; Pais and Hulot 2000; Hulot et al. 2002; Eymin and Hulot 2005), the pattern of streamlines in Fig. 5a are derived by interpreting the changes in the field on the core–mantle boundary as the result of magnetic induction by a time variable, large-scale, mostly horizontal (i.e., tangential) outer core velocity field. Although frozen-flux core flow models are nonunique and are subject to diverse sources of error, including short-lived transients, unresolved small-scale flows, diffusion, crustal filtering, and limited data accuracy, many of the largest structures in Fig. 5a are found in these models, and they tend to be rather persistent over time. Examples of these flow features include the mid- and low-latitude westward motion beneath the Southern Atlantic, equatorward motion beneath the eastern Indian Ocean, westward motion beneath Africa, and the generally poleward motion beneath the western margin of the South Atlantic. Together these flow structures form the large anticyclonic (counterclockwise) gyre that dominates the flow in the southern hemisphere. Typical flow speeds in this gyre are on the order of 10 km year^{-1}, equivalent to a circulation time of about 1.5 ka. Other significant flow features include an anticyclonic (clockwise) gyre below North America and westward polar vortices at both hemispheres.

Analysis of dipole moment change on the core–mantle boundary

We can identify the sources of the observed dipole moment change as they appear on the core–mantle boundary using the following theory for the evolution of the dipole moment produced within a conducting fluid. The dipole moment vector **m** can be expressed in terms of the current density **J** or the magnetic field **B** inside a conductor as:

$$\mathbf{m} = \frac{1}{2}\int \mathbf{r}\times\mathbf{J}dV = \frac{3}{2\mu_0}\int \mathbf{B}dV \qquad (6)$$

where dV denotes volume integration and **r** is the radial position vector. Assuming the conductor is a fluid and

Ohm's law applies, the rate of change of the dipole moment in a sphere can be written (see Moffatt 1978; Davidson 2001) as:

$$\dot{\mathbf{m}} = \frac{3}{2\mu_0}\int \frac{\partial \mathbf{B}}{\partial t}\,dV = \frac{3}{2\mu_0}\int (\mathbf{u}\mathrm{B_r} - \lambda\hat{\mathbf{r}}\times(\nabla\times\mathbf{B}))dS \tag{7}$$

where $\hat{\mathbf{r}}$ is the radial unit vector and dS denotes integration over the surface of the sphere. Because the outer core fluid velocity vanishes at its boundary with the solid mantle, **u** in Eq. 7 is usually interpreted to be the tangential, free-stream velocity beneath the boundary layer that is adjacent to the core–mantle boundary.

We are primarily concerned here with using this theory to interpret the changes in the axial moment. The axial component of Eq. 7 can be written as:

$$\dot{m}_z \equiv \int \dot{\rho}_z dS = -\frac{3}{2\mu_0}\int (u_\theta \sin\theta B_r + \frac{\lambda}{r_c}\frac{\partial(rB_\theta)}{\partial r}\sin\theta - \frac{\lambda}{r_c}\frac{\partial B_r}{\partial\theta}\sin\theta)dS \tag{8}$$

The left hand side of Eq. 8 is just the observed axial moment change expressed as a surface integral of the change in ADM density $\dot{\rho}_z$, which is defined as:

$$\dot{\rho}_z = \frac{3r_c}{2\mu_0}\cos\theta\dot{B}_r \tag{9}$$

Figure 5b shows the distribution of $\dot{\rho}_z$ at 1980 in units of $A\ s^{-1}$. The terms on the right hand side of Eq. 8 denote contributions to $\dot{m}_z$ on or just below the core–mantle boundary, and represent the effects of meridional advection of magnetic field, radial magnetic field diffusion, and meridional magnetic field diffusion, respectively. If the observed dipole moment change were entirely due to diffusion, as in the case of Ohmic-free decay considered earlier, then the sum of the two diffusion terms would equal $\dot{m}_z$ in Eq. 8. Alternatively, if frozen-flux conditions are held exactly everywhere on the core–mantle boundary, then the meridional advection term in Eq. 8 would equal $\dot{m}_z$.

The contribution of meridional diffusion to $\dot{m}_z$ can be calculated using the θ-derivative of the radial core–mantle boundary field shown in Fig. 5a. It is easily shown that meridional diffusion is far too small (by a factor of 30 or more, depending on the choice of magnetic diffusivity λ) to account for the observed $\dot{m}_z$, and can be ignored in our analysis. This is consistent with the interpretation of the rate of Ohmic-free decay of the fundamental dipole mode in the core, and indicates that only meridional advection of magnetic field and radial magnetic diffusion are large enough to account for the observed axial moment changes. The effects of radial magnetic diffusion can be seen indirectly at many places on the core–mantle boundary, most prominently, where the reverse flux spots in Fig. 5a have formed. However, because the radial diffusion term in Eq. 8 involves unknown r-derivatives of the field inside the core, we cannot calculate the radial diffusion effect directly from a map of B_r on the core boundary.

It is possible to estimate the contribution to moment change from advection near the core–mantle boundary. Geometrically, meridional advection acts to reduce the axial moment by transporting outward-directed magnetic flux (positive B_r) toward the north geographic pole and inward-directed magnetic flux (negative B_r) toward the south geographic pole. Places on the core–mantle boundary where advective effects are most active can be identified using a frozen-flux core flow model. Figure 5c shows a map of the integrand of the advective term in Eq. 8, the quantity $-3u_\theta \sin\theta B_r/2\mu_0$ where in this case B_r is the 1980 radial field in Fig. 5a and u_θ is the meridional component of the frozen-flux velocity field at the same time. As Fig. 5c shows, the contribution from frozen-flux advection is very heterogeneous over the core–mantle boundary, strengthening the dipole moment at some locations and weakening it at others with a large amount of cancellation, particularly within individual vortex structures. The largest frozen-flux sources and sinks of dipole moment correspond to places where the core flow crosses the B_r contours with a large meridional (i.e., north–south) component. Beneath North America and the westernmost Atlantic, for example, the western limb of a large clockwise gyre is strengthening the dipole moment by advecting inward-directed field toward the North Pole, while the eastern limb of the same gyre is reducing the dipole moment by advecting inward-directed field away from the North Pole. The two limbs of the clockwise gyre beneath East Asia also generate a source–sink pair, as do the two limbs of the vortex beneath Central Africa. The net effect on the ADM of these two northern hemisphere vortices is quite small, however, because the sources and sinks tend to cancel. This is consistent with the results in Fig. 4e,f, which show that the northern hemisphere contributes little to the dipole moment change.

In contrast to the situation in the northern hemisphere, frozen-flux flow in the southern hemisphere has a far larger influence on the ADM change. Figure 5a shows the eastern limb of the main counterclockwise gyre advecting a large lobe of outward-directed field from below Antarctica toward the equator below the Indian Ocean, roughly along the 90°E meridian. This is the most persistent unbalanced advective sink of axial moment over the last 150 years, and is the largest advective sink in the southern hemisphere in 1980, as indicated in Fig. 5c. It contributes more than one half of that hemisphere's frozen-flux dipole moment decrease rate at 1980, and about one half of the global total. Figure 5a–c reveals the spatial relationships between B_r, the moment density change $\dot{\rho}_z$, and the advective contribution

to $\dot{m}_z$ in this region. Figure 5b shows that the center of moment density change lies beneath the Antarctic coast, on the western margin of the high-intensity flux spot seen in Fig. 5a where the meridional velocity is large and directed toward the equator. Comparison of subpanels b and c of Fig. 5 indicates that the advective transport is located downstream of the center of $\dot{\rho}_z$ in this region. Overall, frozen-flux advection accounts for about 80% of the observed $\dot{m}_z$ at 1980. Figure 5d shows the global advective contribution to ADM change between 1840 and 1990 according to our frozen-flux flow model, compared with the observed moment change $\dot{m}_z$ for the same time interval. We also show the *reduced* moment change obtained by integrating $\dot{\rho}_z$ in Fig. 5b with reversed flux regions omitted. A range of frozen-flux calculations are shown in Fig. 5d, corresponding to different values of the parameter k, the ratio of surface divergence to radial vorticity in our model (Amit and Olson 2006). Small values of k result in less streamline diffusion and overall larger fluid velocities. The moment change associated with frozen-flux advection shows a pattern of variation similar to the observed $\dot{m}_z$ with some suggestion of a phase lag in the early and middle portions of the 20th century. In terms of magnitude, the time-averaged advective contribution in models with small k values is about 67% of the observed change, and since 1970 these same models account for nearly 80% of the observed change.

Attempts to constrain the frozen-flux flow to exactly satisfy the observed $\dot{m}_z$ resulted in a large misfit with the other harmonics of the secular variation, the size of the misfit scaling with the unexplained moment change in Fig. 5d. As remarked previously, frozen-flux core flow models are inherently uncertain due to errors in the data, crustal filtering, unseen small-scale flows, and other effects stemming from their finite resolution (Bloxham and Jackson 1991). More importantly in this context, however, is the fact that the frozen-flux assumption ignores radial magnetic diffusion. Previous studies have found that frozen-flux core flow models commonly underestimate the secular variation of the axial dipole (Jackson 1997; Whaler and Davis 1997), a bias that has already been ascribed to diffusion (Holme and Olsen 2006). A similar bias might be present in this case as well. Most of the discrepancy in Fig. 5d between observed and calculated moment changes is a result of the contribution from growth of reversed flux patches. The insert plot in Fig. 5d shows that the frozen-flux advection has nearly the same amplitude as the reduced $\dot{m}_z$ for small k values. Furthermore, the contribution to frozen-flux advection that comes from reversed flux patch motion is minimal. As seen in Fig. 5a,c, reverse flux patches do not coincide with strong meridional flow and subtracting their contributions hardly changes the model curves in Fig. 5d. Reversed flux patch formation and growth are evidence for radial magnetic diffusion, possibly combined with smaller scale advective effects that are unresolved in the core field models. It is therefore possible that frozen-flux advection basically accounts for the observed axial moment change since 1840 except for the part due to reverse flux patch growth, which is diffusive in origin.

The above analysis suggests how the interplay between diffusion and advection can induce a rapid yet sustained decrease in dipole moment. First, convection transports magnetic field lines upward from deeper in the outer core, inducing radial gradients in the magnetic field below the core–mantle boundary. Radial diffusion then acts on these magnetic boundary layer structures, inducing rapid changes of the field on the core–mantle boundary and creating reversed flux patches in some places (emergence of reversed flux is an obvious sign of diffusion, but diffusion acts on normal flux as well). The large-scale circulation in the core then redistributes the magnetic flux over the core–mantle boundary.

In this scenario, radial magnetic diffusion plays a crucial but largely invisible role in changing the dipole moment as seen on the core–mantle boundary. Fluid motion below the core–mantle boundary sustains the boundary layer-type magnetic flux distribution that allows the rapid outward diffusion of the field to occur, and it transports flux over the core–mantle boundary. Applying this interpretation to the trends shown in Fig. 5d suggests that the current episode of dipole moment decrease will continue for some time into the future. According to our analysis, the influence of advection was in roughly constant proportion to the observed moment change at least for the past century. This supports the inference that diffusion and advection are working together, and the rapid moment decrease we are experiencing today is likely to persist until the geodynamo substantially alters the arrangement. Finally, we remark that the capacity for a *very* large moment decrease under present conditions may be somewhat limited. Relatively little magnetic flux crosses the equator, and the frozen-flux core flow consists mostly of recirculating vortices with a strong tendency for advective cancellation.

Rapid dipole moment decrease in a numerical dynamo

The geomagnetic field and its secular variation delineate regions on the core–mantle boundary where dipole moment changes are occurring, regions where frozen-flux transport effects are large (both positive and negative), and help identify regions where radial diffusion is active. But there are limits to how accurately we can measure the strength of these mechanisms and, in any case, the picture is incomplete because the moment analysis

applies only to the neighborhood of the core–mantle boundary. However, the geodynamo is a three-dimensional process with magnetic field generation taking place throughout the outer core. Important pieces of information on the field inside the core that are needed to fully understand dipole moment change are not accessible to us. For example, theory dictates that a principal component of the geomagnetic field, the toroidal component, has little or no surface manifestation, yet plays a crucial role in the dynamo process (Bloxham 1986; Glatzmaier and Roberts 1995; Glatzmaier et al. 1999; Christensen et al. 1999; Kageyama et al. 1999; Olson et al. 1999; Sarson and Jones 1999; Buffett 2000; Jones 2000; Kutzner and Christensen 2002; Wicht and Olson 2004; Glatzmaier and Olson 2005) and may play a significant role in the current dipole moment decrease. Accordingly, geomagnetic field phenomena on the core–mantle boundary are symptoms of the more fundamental, three-dimensional processes at work in the core's interior. The problem then is how to diagnose these dynamo processes from their surface symptoms.

One approach is to exploit the recent advances in numerical modeling of self-sustaining fluid dynamos. The past decade has witnessed huge strides in the ability to model the dynamo process numerically, starting from the equations of magnetohydrodynamics (Busse 2000; Dormy et al. 2000; Glatzmaier 2002; Kono and Roberts 2002). A major advantage of this approach is its self-consistency. Numerical dynamos simultaneously solve the time-dependent induction equation for the magnetic field plus the Navier–Stokes equation for the fluid motion and transport equations for buoyant constituents in the rotating spherical geometry of the core (Zhang and Busse 1989; Glatzmaier and Roberts 1995; Kuang and Bloxham 1997; Olson et al. 1999; Grote et al. 2000; Kutzner and Christensen 2002; Takahashi et al. 2005). The main drawback of these models is their inability to reach the correct parameters for the geodynamo. In particular, the numerical models must assume too large values for the fluid viscosity and thermal and chemical diffusivities relative to other physical parameters. This makes the dynamo models more diffusive (less turbulent) than the actual core, particularly with respect to diffusion of momentum and buoyancy (Simitev and Busse 2005). At the present time we do not have a complete picture of all the ramifications these shortcomings entail. Even so, numerical dynamos have had some remarkable success. For example, they provide an explanation for the low order part of the core field, especially the dominant axial dipole, in terms of the style of convection in the core (Dormy et al. 2000; Kono and Roberts 2002). They also exhibit many forms of secular variation, including realistic-looking polarity reversals in some cases (Glatzmaier et al. 1999; Kageyama et al. 1999; Sarson and Jones 1999; Kutzner and Christensen 2002; Wicht and Olson 2004; Takahashi et al. 2005).

Figures 6 and 7 show images of a numerical dynamo model with time variable dipole moment, which exhibits episodes of rapid dipole moment decrease. This dynamo model is driven by thermal convection in a rotating, electrically conducting Boussinesq fluid in a spherical shell with the same geometry (inner/outer core radius ratio) as the Earth. Control parameters are Rayleigh number $Ra=6.5 \times 10^5$, Ekman number $E=4 \times 10^{-4}$, Prandtl number Pr=1, and magnetic Prandtl number Pm=5. Details of the numerical dynamo model used in this example are described in Christensen et al. (1999).

The magnetic field in this particular model is dominated by the axial dipole component. The ADM fluctuates on both long and short periods with amplitude variations up to 50%. No polarity reversals occurred during this simulation

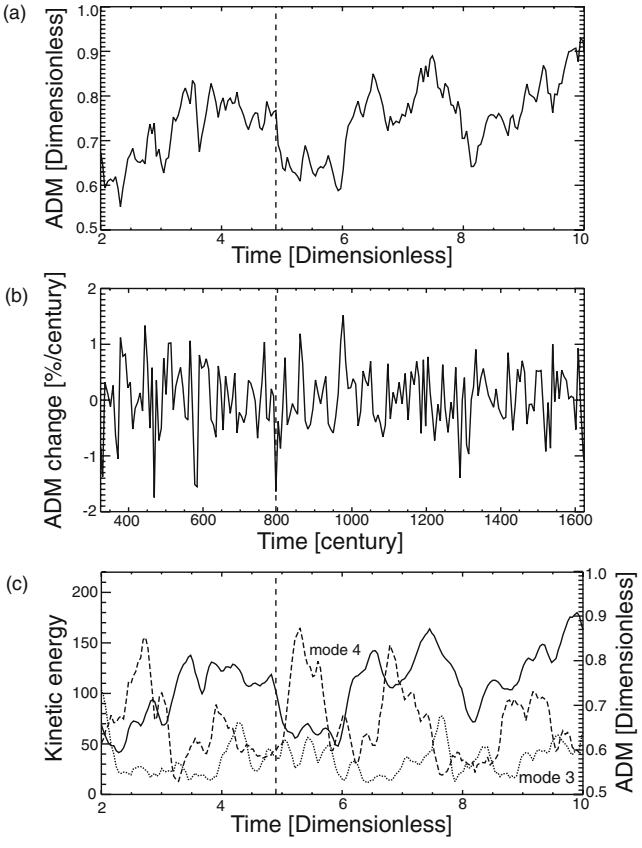

Fig. 6 Axial dipole moment (*ADM*) decrease event in a numerical dynamo model. The dynamo model is driven by thermal convection in a rotating, electrically conducting spherical shell of fluid with the same geometry as the Earth's core. Control parameters are Rayleigh number $Ra=6.5 \times 10^5$, Ekman number $E=4 \times 10^{-4}$, Prandtl number Pr=1, and magnetic Prandtl number Pm=5. **a** Time series of ADM decrease event marked by *dashed line*. **b** Time series of ADM rate of change, assuming an electrical conductivity of $\sigma = 4 \times 10^5\ Sm^{-1}$ (corresponding to a magnetic diffusivity of $\lambda = 2\ m^2 s^{-1}$). **c** Time series of kinetic energy in convective azimuthal modes 3 (*dotted*) and 4 (*dashed*) and smoothed ADM (*solid*)

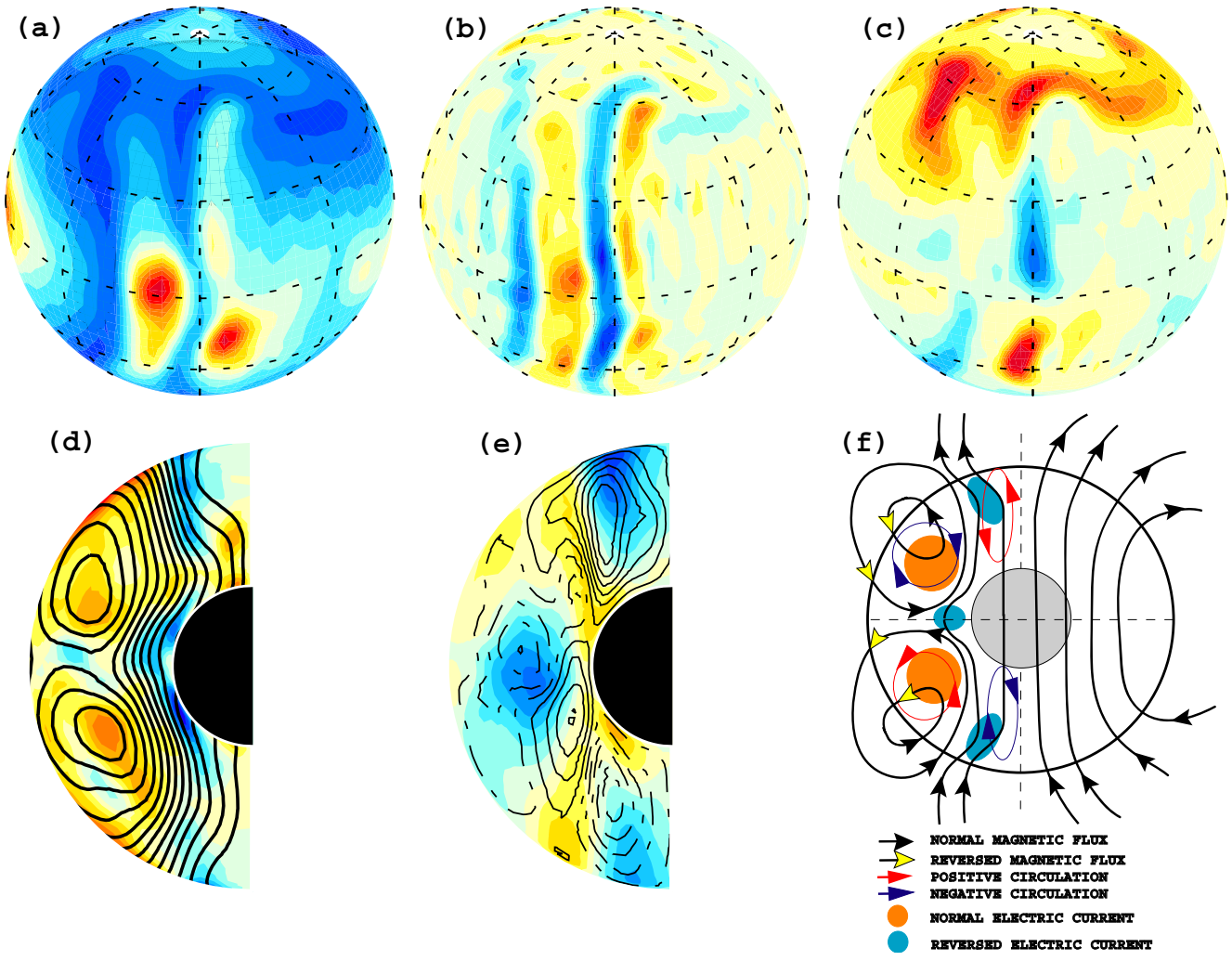

Fig. 7 Snapshot images of the dynamo model during the moment decrease event: *red contours* = positive values and *blue contours* = negative values. **a** Heat flow on the core–mantle boundary. **b** Radial fluid velocity just below the core–mantle boundary. **c** Radial magnetic field on the core–mantle boundary. **d** Cross-section of zonal azimuthally averaged (east–west) electric current density (*filled contours*) with zonal azimuthally averaged poloidal magnetic field *lines superimposed*. **e** Cross-section of zonal azimuthally averaged (east–west) fluid velocity (*filled contours*) with meridional streamlines superimposed. **f** Illustration of convective circulation (*left*) interacting with a simple axial dipole field (*right*), inducing reverse electric currents in the core, reverse magnetic field on the core–mantle boundary, and axial moment decrease

and it is uncertain if the moment fluctuations seen here would lead to an occasional reversal. The polarity shown in Fig. 7 happens to be the reverse of the present-day geomagnetic field polarity, a consequence of the initial conditions of the calculation, although the dipole polarity has no effect on the dynamics. This model was chosen because it exhibits a number of properties that may be considered "Earth-like" despite being far from the Earth in physical parameter space. Its ADM comes mainly from a few (2–4) high latitude high-intensity flux spots in each hemisphere. It has a magnetic spectrum similar to the geomagnetic field and the slope of its secular variation spectrum is comparable to the slope of geomagnetic secular variation spectrum. The scale of flow (azimuthal modes 3, 4, and 5 dominate) is commensurate with the scale of core flow imaged by the frozen-flux methods described previously. The flow speeds in this model are smaller than in Fig. 5, roughly by a factor of five, as is the magnitude of the magnetic secular variation. These scaling differences are due to the fact that the magnetic Reynolds number in this model is smaller by the same factor of five than estimated for the Earth's core (Christensen and Tilgner 2004).

The snapshots of the radial magnetic field, radial velocity, surface heat flow at or just below the core–mantle boundary, and zonal (azimuthal average) sections of azimuthal current, magnetic field, and velocity (Fig. 7) correspond to the dipole moment decrease event indicated by the dashed line in the time series plots (Fig. 6). During this event, the ADM fell by about 23% at a peak rate of 1.6% per century based on an assumed magnetic diffusivity

of 2 $m^2 s^{-1}$. The origin of this event can be seen in Fig. 6c, which compares a smoothed version of the ADM variations with time series of fluid kinetic energy in azimuthal modes 3 and 4, the dominant convective modes. The convective structure vacillates between two states, one with mixed modes and the other dominated by mode 4. The dipole moment decrease coincides with a transition to the mode 4 state, which is evidently less efficient as a dynamo. Similar transitions can be seen in other parts of the time series.

The effect of the flow transition can be seen in the snapshots in Fig. 7, particularly in the radial magnetic field, which shows several reversed flux spots forming at midlatitudes above a sector with enhanced convective activity. These reversed flux spots first appear early in the dipole decrease event and coincide with the change in the convective style. Because they are associated with a flow transition, the high-latitude reversed flux patches are most evident when the dipole is relatively strong before the moment decrease event. Paradoxically perhaps, the periods with weakest dipole moment in this model are characterized by relatively little reversed flux.

The relationship between azimuthal electric currents and convective velocity in the dynamo interior tells a similar story. According to Eq. 6, positive azimuthal current enhances and negative azimuthal current reduces the ADM in this model so that changes in the relative strength of the positive and negative current distributions shown in Fig. 7d are equivalent to changes in the ADM. The positive electric currents in Fig. 7d are mostly generated by the nonaxisymmetric convection outside the tangent cylinder of the inner core. The reversed currents are mostly generated near the inner core tangent cylinder in the outflow from the polar plumes and in the equatorial upwelling, all evident in the meridional circulation in Fig. 7e. Reversed electric current regions are relatively strong after a flow transition because magnetic field lines are distorted by newly formed upwellings and downwellings. Where the field lines transported upward in a convective upwelling reach the outer boundary, magnetic reconnection occurs as illustrated in Fig. 7f above the equatorial upwelling. Enhanced radial diffusion and reversed flux patch formation occurs at these locations as shown, for example, in the convectively active sector in Fig. 7a–c.

The various contributions to ADM decrease in the event shown in Figs. 6 and 7 can be analyzed using Eq. 8, as in this case, all the input quantities are known with adequate precision from the dynamo model. The interaction between transverse advection and radial diffusion on the boundary of this dynamo model is qualitatively consistent with our interpretation in the previous section of the geomagnetic field behavior during the present-day dipole moment decrease event. For example, meridional advection and radial diffusion are the dominant mechanisms below the Ekman boundary layer, contributing about 40% and 50% to the ADM decrease, respectively, whereas meridional diffusion is secondary, contributing only 10%. Preliminary results indicate that rapid dipole moment changes in dynamo models involve both advective and diffusive contributions in roughly comparable amounts, provided the magnetic Reynolds number is large. However, this phenomenon is far from being fully understood and deserves systematic numerical study.

Speculations on the future

The recent history of the geomagnetic field indicates that reversed magnetic flux proliferation combined with weakening and equatorward motion of the high-intensity normal polarity flux patches on the core–mantle boundary may continue into the future with further erosion of the dipole moment. How long this will continue is uncertain, but even a modest continuation of the present trends can have practical consequences if, for example, the SAA source on the core–mantle boundary continues to extend by growth of reversed flux regions beneath South America, Southern Africa, and Antarctica.

The location of the SAA in the more distant future depends on the development of these features on the core–mantle boundary, plus the evolution of the intense normal polarity field patches that control the location of the equatorial dipole. Over the past century, the intense normal field patches below Australia and the Indian Ocean have exerted the most control on the equatorial dipole, fixing its location in the eastern hemisphere. We have argued that the existence and location of the SAA is partly attributable to reverse flux patches in the southern hemisphere. The large gyre in the southern hemisphere core flow transports high-intensity normal polarity field toward the equator below the Indian Ocean and reverse field westward toward beneath South America. So long as this circulation continues to have this effect, the conditions that produce the SAA—reverse flux in the west and intense normal flux in the east—are likely to prevail in the southern hemisphere.

There is some evidence suggesting this situation is beginning to change. The geomagnetic tilt, which had been nearly constant for more than a century, has diminished since 1970 despite the rapid decrease in the GADM. Another indication of change is the spot of reversed flux can be seen in its infancy below the subequatorial North Atlantic. This feature has evidently developed within the past 30 years and is growing as it drifts toward the Caribbean. If it continues to develop and if the NGP continues its current trajectory, passing over the north geographic pole, the stage would be set for a new magnetic structure on the core–mantle boundary, a North Atlantic Anomaly.

What about the next reversal? Is the present episode of dipole decrease a prelude to a full polarity change? The last full reversal occurred around 785 ka, a long time compared with the 240 ka average period of polarity chrons over the past 5 Ma. However, today's large dipole moment indicates that the processes in the core, which could lead to a polarity reversal, were not active long enough for a reversal to be imminent, in spite of the currently rapid moment decrease. It is more likely that this event is another one of the many dipole moment fluctuations in evidence throughout the paleomagnetic record. But even if the present-day episode is just a part of a fluctuation, it is well worth understanding its underlying physical processes because these are likely the same processes that cause reversals when they occur.

Perhaps we should ask a different question: What would it take for the current event to develop into a full polarity reversal? According to Maxwell's equations, a dipole polarity change corresponds to reversal of the main azimuthal electric current system in the core. Reversed magnetic flux patches are one symptom of reversed electric currents lying below the core–mantle boundary. Suppose that a perturbation in the convection generates a localized region somewhere deep in the core with reversed electric currents and reversed magnetic flux on the core–mantle boundary, similar to the ones shown in Fig. 7c. Ordinarily, such perturbations will be subcritical, too small to grow on their own, capable of temporarily diminishing the dipole, but not reverse it. However, suppose this perturbation with its reversed electric currents is located in a region of the core where the convection is particularly energetic. In this situation the local magnetic Reynolds number based on the size and velocity of the perturbation might exceed the critical value for regeneration. The perturbation could then transition from benign to malignant, able to grow by drawing energy from the normal polarity field around it. Such malignant growth is often seen in numerical dynamo models with reversals (Glatzmaier et al. 1999; Kutzner and Christensen 2000, 2002). In other models, similar growing perturbations take the form of propagating diffusive magnetic disturbances called dynamo waves (Wicht and Olson 2004; Takahashi et al. 2005).

Regardless of the internal mechanisms, surface expression of a dynamo perturbation at depth includes proliferation of reversed flux patches on the core–mantle boundary, and in particular, reversed flux patches at middle and high latitudes (reversed flux near the equator has little effect on the ADM and is generally not an indication of a major perturbation to the dynamo). Following up an early suggestion by Cox (1975), Gubbins (1987) proposed that the reversed flux patch growth observed at middle latitudes in the southern hemisphere of the core–mantle boundary over the past century is an indication of the polarity reversal process at work. In this connection, the evidence for new middle and high latitude reversed flux patches in the Ørsted and CHAMP satellite core fields model are especially intriguing. We anticipate that a full understanding of this phenomenon will emerge from improvements in our ability to model the geodynamo numerically, coupled with better spatial and temporal resolution of the core field using satellite measurement programs such as the planned SWARM constellation.

Acknowledgements We acknowledge the support of the Geophysics Program of the National Science Foundation. Johannes Wicht made numerous helpful suggestions, as did several anonymous referees.

References

Amit H, Olson P (2004) Helical core flow from geomagnetic secular variation. Phys Earth Planet Inter 147:1–25

Amit H, Olson P (2006) Time-average and time-dependent parts of core flow. Phys Earth Planet Inter 155:120–139

Backus G, Parker R, Constable C (1996) Foundations of geomagnetism. Cambridge University Press, Cambridge

Badhwar GD (1997) Drift rate of the South Atlantic anomaly. J Geophys Res 102:2343–2349

BEIR VII Phase 2 (2005) Health risks from exposure to low levels of ionizing radiation. The National Academy Press, Washington DC

Benton ER, Voorhies CV (1987) Testing recent geomagnetic field models via magnetic flux conservation at the core–mantle boundary. Phys Earth Planet Inter 48:350–357

Biggin AJ, Thomas DN (2003) Analysis of long-term variations in the geomagnetic poloidal field intensity and evaluation of their relationship with global geodynamics. Geophys J Int 152: 392–415

Birk GT, Lesch H, Konz C (2004) Solar wind induced magnetic field around the unmagnetized Earth. Astron Astrophys 420:L15–L18

Bloxham J (1986) The expulsion of magnetic flux from the Earth's core. Geophys J R Astron Soc 87:669–678

Bloxham J (1989) Simple models of fluid flow at the core surface derived from geomagnetic field models. Geophys J Int 99: 173–182

Bloxham J (1992) The steady part of the secular variation of the Earth's magnetic field. J Geophys Res 97:19565–19579

Bloxham J, Jackson A (1991) Fluid flow near the surface of Earth's outer core. Rev Geophys 21:97–120

Bloxham J, Jackson A (1992) Time-dependent mapping of the magnetic field at the core–mantle boundary. J Geophys Res 97:19565–19579

Bloxham J, Gubbins D, Jackson A (1989) Geomagnetic secular variation. Philos Trans R Soc London A 329:415–502

Bogue SW, Paul HA (1993) Distinctive field behavior following geomagnetic reversals. Geophys Res Lett 20:2399–2402

Bottollier-Depois JF, Chau Q, Bouisset P, Kerlau G, Plawinski L, Lebaron-Jacobs L (2000) Assessing exposure to cosmic radiation during long-haul flights. Radiat Res 153(5 Pt 1):526–532

Brasseur G, Solomon S (1984) Aeronomy of the middle atmosphere. Reidel, Boston

Buffett BA (1992) Constraints on magnetic energy and mantle conductivity from the forced nutation of the Earth. J Geophys Res 97:18581–19597

Buffett BA (2000) Earth's core and the geodynamo. Science 288:2007–2012
Buhler P, Desorgher L, Zehnder A, Daly E, Adams L (1996) Observations of the low Earth orbit radiation environment from Mir. Radiat Meas 26:917–921
Bullard EC, Freedman C, Gellman H, Nixon J (1950) The westward drift of the Earth's magnetic field. Philos Trans R Soc Lond A 243:67–92
Busse FH (2000) Homogeneous dynamos in planetary cores and in the laboratory. Annu Rev Fluid Mech 32:383–408
Busse FH, Grote E, Simitev R (2003) Convection in rotating spherical shells and its dynamo action. In: Jones CA, Soward AM, Zhang K (eds) Earth's core and lower mantle. Taylor and Francis, London
Cain JC, Wang Z, Schmitx DR, Meyer J (1989) The geomagnetic spectrum for 1980 and core-crustal separation. Geophys J Int 97:443–447
Carlowicz MJ, Lopez RE (2002) Storms from the sun. Joseph Henry Press, Washington DC
Carlut J, Courtillot V (1998) How complex is the time-averaged geomagnetic field over the past 5 myr? Geophys J Int 134:527–544
Carlut J, Courtillot V, Hulot G (2000) Over how much time should the geomagnetic field be averaged to obtain the mean paleomagnetic field? Terra Nova 11:39–243
Chapman S, Bartels J (1962) Geomagnetism, vols. I and II. Oxford University Press, Oxford UK
Christensen U, Tilgner A (2004) Power requirement of the geodynamo from ohmic losses in numerical and laboratory dynamos. Nature 439:169–171
Christensen U, Olson P, Glatzmaier GA (1999) Numerical modeling of the geodynamo: a systematic parameter study. Geophys J Int 138:393–409
Clement BM (2004) Dependence of the duration of geomagnetic polarity reversals on site latitude. Nature 428:637–640
Constable CG (2003) Geomagnetic reversals. In: Jones CA, Soward AM, Zhang K (eds) Earth's core and lower mantle. Taylor and Francis, London
Constable CG, Johnson CL (2005) A paleomagnetic power spectrum. Phys Earth Planet Inter 153:61–73
Constable CG, Korte M (2005) Is Earth's magnetic field reversing? Earth Planet Sci Lett 236:348
Constable CG, Parker RL (1988) Statistics of geomagnetic secular variation for the past 5 m.y. J Geophys Res 93:11569–11581
Constable CG, Johnson CL, Lund SP (2000) Global geomagnetic field models for the past 3000 years: transient or permanent flux lobes? Philos Trans R Soc London A 358:991–1008
Courtillot V, Besse J (1987) Magnetic field reversals, polar wander, and core–mantle coupling. Science 237:1140–1147
Cox A (1975) Reversed flux as reversal mechanism. Rev Geophys Space Phys 13:35–51
Davidson PA (2001) Introduction to magnetohydrodynamics. Cambridge University Press, Cambridge
DeSantis A, Barraclough DR, Tozzi R (2003) Spatial and temporal spectra of the geomagnetic field and their scaling properties. Phys Earth Planet Inter 135:125–134
De Wijs GA (1998) The viscosity of liquid iron at the physical conditions of the Earth's core. Nature 392:805–807
Deme S, Reitz G, Apthy I, Hjja I, Lng E, Fehr I (1999) Doses due to the South Atlantic anomoly during the Euromir'95 mission measured by an on-board TLD system. Radiat Prot Dosim 85:301–304
Dobson DP, Crichton WA, Vocadlo L, Jones AP, Wang Y, Uchida T, Rivers M, Sutton S, Brodholt JP (2000) In situ measurement of viscosity of liquids in the Fe–FeS system at high pressures and temperatures. Am Mineral 85:1838–1842
Dormy E, Valet JP, Courtillot V (2000) Numerical models of the geodynamo and observational constraints. Geochem Geophys Geosyst 1(10). DOI 10.1029/2000GC000062
Durante M (2002) Biological effects of cosmic radiation in low-Earth orbit. Int J Mod Phys A 17:1713–1721
Dziewonski AM, Anderson DL (1981) Preliminary reference Earth model. Phys Earth Planet Inter 25:297–356
Eymin C, Hulot G (2005) On surface core flows inferred from satellite magnetic data. Phys Earth Planet Inter 152:200–220
Fraser-Smith AC (1987) Centered and eccentric geomagnetic dipoles and their poles 1600–1985. Rev Geophys 25:1–16
Gauss CF (1877) Allgemeine Theorie des Erdmagnetismus. Werke 5:121–193 (original publication in 1839, Weidmann, Leipzeg; translated into English by Sabine E and edited by Taylor R in Scientific Memoirs, vol. 2 in 1841, Taylor and Taylor, London)
Gee J, Conde SC, Hildebrand JA, Donnelly JA, Parker RL (2000) Geomagnetic intensity variations over the past 780 kyr obtained from near-seafloor anomalies. Nature 408:827–832
Gire C, LeMouël J-L (1990) Tangentially geostrophic flow at the core–mantle boundary compatible with the observed geomagnetic secular variation: the large-scale component of the flow. Phys Earth Planet Inter 59:259–287
Gire C, LeMouël J-L, Madden T (1986) Motions of the core surface derived by SV data. Geophys J R Astron Soc 84:1–29
Glatzmaier GA (2002) Geodynamo simulations—how realistic are they? Annu Rev Earth Planet Sci 30:237–257
Glatzmaier GA, Olson P (2005) Probing the geodynamo. Sci Am 292:50–57
Glatzmaier GA, Roberts PH (1995) A three-dimensional convective dynamo solution with rotating and finitely conducting inner core and mantle. Phys Earth Planet Inter 91:63–75
Glatzmaier GA, Coe RS, Hongre L, Roberts PH (1999) The role of the mantle in controlling the frequency of geomagnetic reversals. Nature 401:885–890
Glassmeier KH, Vogt A, Stadelmann Z, Buchert S (2004) Concerning long-term geomagnetic variations and space climatology. Ann Geophys 22:3669–3677
Golightly MJ, Hardy K, Quam W (1994) Radiation dosimetry during US space shuttle missions with the RME-III. Radiat Meas 23:25–42
Grote E, Busse FH, Tilgner A (2000) Convection-driven quadrupole dynamos in rotating spherical shells. Phys Rev E Stat Phys Plasmas Fluids Relat Interdiscip Topics 60:5025–5028
Gubbins D (1982) Finding core motions from magnetic observations. Philos Trans R Soc Lond A 306:249–256
Gubbins D (1987) Mechanism for geomagnetic polarity reversals. Nature 326:167–169
Gubbins D (1999) The distinction between geomagnetic excursions and reversals. Geophys J Int 137:F1–F3
Gubbins D (2004) Time series analysis and inverse theory for geophysicists. Cambridge University Press, Cambridge
Gubbins D, Jones AL, Finlay C (2006) Fall in Earth's magnetic field is erratic. Science 321:900–903
Gundestrup M, Storm HH (1999) Radiation induced acute myeloid leukaemias and other cancers in commercial jet cockpit crew: a population based cohort study. Lancet 354:2029–2031 (Dec 11)
Guyodo Y, Valet JP (1999) Global changes in geomagnetic intensity during the past 800 thousand years. Nature 399:249–252
Hale CJ (1987) Paleomagnetic data suggest a link between the Archaean–Proterozoic boundary and inner-core nucleation. Nature 329:233–237
Hale CJ, Dunlop DJ (1987) The intensity of the geomagnetic field at 3.5 Ga: paleointensity results from the Komati formation, Barberton Mountain Land, South Africa. Earth Planet Sci Lett 86:354–364

Hargreaves JK (1992) The solar-terrestrial environment: an introduction to geospace—the science of the terrestrial upper atmosphere, ionosphere, and magnetosphere. Cambridge University Press, New York

Heirtzler JR (2002) The future of the South Atlantic anomaly and implications for radiation damage in space. J Atmos Solar Terr Phys 64:1701–1708

Heller R, Merrill RT, McFadden PL (2003) Two states of paleomagnetic intensities for the past 320 million years. Phys Earth Planet Inter 135:211–223

Holme R (1998) Electromagnetic core–mantle coupling-I. Explaining decadal changes in the length of day. Geophys J Int 132:167–180

Holme R, Olsen N (2006) Core-surface flow modelling from high resolution secular variation. Geophys J Int (in press). DOI 10.1111/j1365-246X.2006.03033.x

Holme R, Whaler KA (2001) Steady core flow in an azimuthally drifting reference frame. Geophys J Int 14:560–569

Hulot G, Eymin C, Langlais B, Mandea M, Olsen N (2002) Small-scale structure of the geodynamo inferred from Ørsted and Magsat satellite data. Nature 416:620–623

Jackson A (1997) Time-dependency of tangentially geostrophic core surface motions. Phys Earth Planet Inter 103:293–311

Jackson A (2003) Intense equatorial flux spots on the surface of the Earth's core. Nature 424:760–763

Jackson A, Bloxham J, Gubbins D (1993) Time-dependent flow at the core surface and conservation of angular momentum in the coupled core–mantle system. In: LeMouël J-L, Smylie DE, Herring T (eds) Dynamics of Earth's deep interior and Earth rotation, Geophys Monogr 12(72):97–107

Jackson A, Jonkers ART, Walker MR (2000) Four centuries of geomagnetic secular variation from historical records. Philos Trans R Soc Lond A 358:957–990

Jacobs JA (1984) Reversals of the Earth's magnetic field. Adam Hilger, Bristol, UK

Jault D, Gire C, LeMouël J-L (1988) Westward drift, core motions and exchange of angular momentum between core and mantle. Nature 333:353–356

Johnson CL, Constable CG (1997) The time averaged geomagnetic field: global and regional biases for 0–5 Ma. Geophys J Int 131:643–666

Johnson CL, Constable CG, Tauxe LT (2003) Mapping long-term changes in Earth's magnetic field (perspective article). Science 300:2044–2045

Jones CA (2000) Convection-driven geodynamo models. Philos Trans R Soc Lond A 358:873–897

Jonkers ART, Jackson A, Murray A (2003) Four centuries of geomagnetic data from historical records. Rev Geophys 41 (2):11–36

Juarez MT, Tauxe L (2000) The intensity of the time-averaged geomagnetic field: the last 5 Myr. Earth Planet Sci Lett 175: 169–180

Juarez MT, Tauxe L, Gee JS, Pick T (1998) The intensity of the Earth's magnetic field over the last 160 million years. Nature 394:878–881

Kageyama A, Ochi M, Sato T (1999) Flip-flop transition of the magnetic intensity and polarity reversals in the magnetohydrodynamic dynamo. Phys Rev Lett 82:5409–5412

Kono M, Roberts PH (2002) Recent geodynamo simulations and observations of the geomagnetic field. Rev Geophys 40(4):1013

Kono M, Tanaka H (1995) Intensity of the geomagnetic field in geological time: a statistical study. In: Yukutake T (ed) The Earth's central part: its structure and dynamics. Terrapub, Toyko, pp 75–94

Konradi A, Badhwar GD, Braby LA (1994) Recent space shuttle observations of the South Atlantic anomaly and radiation belt models. Adv Space Res 14:911–921

Korte M, Constable CG (2005) Continuous geomagnetic field models for the past 7 millennia: 2. CALS7K. Geochem Geophys Geosyst 6(2). DOI 10.1029/2004GC000801

Kuang W, Bloxham J (1997) An earth-like numerical dynamo model. Nature 389:371–374

Kutzner C, Christensen U (2000) Effects of driving mechanisms in geodynamo models. Geophys Res Lett 27:29–32

Kutzner C, Christensen U (2002) From stable dipolar to reversing numerical dynamos. Phys Earth Planet Inter 131:29–45

Langel RA, Hinze WJ (1998) The magnetic field of the Earth's lithosphere: the satellite perspective. Cambridge University Press, New York

Langel RA, Estes RH, Mead GD, Fabiano EB, Lancaster ER (1980) Initial geomagnetic field model from Magsat vector data. Geophys Res Lett 7:793–796

Larson RL, Olson P (1991) Mantle plumes control magnetic reversal frequency. Earth Planet Sci Lett 107:437–447

Lean J (2005) Living with a variable sun. Phys Today 58(6):32–38

Leaton BR, Malin SRC (1967) Recent changes in the magnetic dipole moment of the earth. Nature 213:1110

Lin JL, Verosub KL, Roberts PA (1994) Decay of the virtual dipole moment during polarity transitions and geomagnetic excursions. Geophys Res Lett 21:525–528

Livermore RA, Vine FJ, Smith AG (1984) Plate motions and the geomagnetic field II. Jurassic to tertiary. Geophys J R Astron Soc 79:939–961

Loper D, McCartney K (1986) Mantle plumes and the periodicity of magnetic field reversals. Geophys Res Lett 13:1525–1528

Malin SRC (1982) Sesquicentenary of Gauss's first measurement of the absolute value of magnetic intensity. Philos Trans R Soc Lond A 306:5–8

Maus S, Rother M, Holme R, Luhr H, Olsen N, Haak V (2002) First scalar magnetic anomaly map from CHAMP satellite data indicates weak lithospheric field. Geophys Res Lett 29:1702–1705

Maus S, Luhr H, Balasis G, Rother M, Mandea M (2004) Introducing POMME, the Potsdam magnetic model of the Earth in CHAMP. In: Reigber C, Lühr H, Schwintzer und P, Wickert J (eds) Earth observation with CHAMP, results from three years in orbit. Springer, Berlin Heidelberg New York, pp 293–298

Maus S, Rother M, Hemant K, Luhr H, Kuvshinov A, Olsen N (2005) Earth's crustal magnetic field determined to spherical harmonic degree 90 from CHAMP satellite measurements. Geophys J Int (in press). DOI 10.1111/j.1365-246X.2006.02833x

McCormack PD, Swenberg CE, Bücker H (eds) (1988) Terrestrial space radiation and its biological effects. NATO ASI series, series A: life sciences, vol 154. Plenum, New York

McDonald KL, Gunst RH (1968) Recent trends in the Earth's magnetic field. J Geophys Res 73:2057–2067

McElhinny MW, Senanayake WE (1982) Variations in the geomagnetic dipole 1. The past 50,000 years. J Geomagn Geoelectr 34:39–51

McFadden PL, Merrill RT (1997) Sawtooth paleointensity and reversals of the geomagnetic field. Phys Earth Planet Inter 103: 247–252

Merrill RT, McFadden PL (1999) Geomagnetic polarity transitions. Rev Geophys 37:201–226

Merrill RT, McElhinny MW, McFadden PL (1998) The magnetic field of the Earth. Academic, San Diego

Moffatt HK (1978) Magnetic field generation in electrically conducting fluids. Cambridge University Press, Cambridge

Mouritsen H, Feenders G, Liedvogel M, Kropp W (2004) Migratory birds use head scans to detect the direction of the earth's magnetic field. Curr Biol 14:1946–1949

Murakami M, Hirose K, Kawamura K, Sata N, Ohishi Y (2004) Post-perovskite phase transition in $MgSiO_3$. Science 304:855–857

Ohno M, Hamano Y (1992) Geomagnetic poles over the past 10,000 years. Geophys Res Lett 19:1715–1718

Olsen N, Holme R, Hulot G, Sabaka T, Neubert T, Toeffner-Clausen L, Primdahl F, Joergensen J, Leger J-M, Barraclough D, Bloxham J, Cain J, Constable C, Golovkov V, Jackson A, Kotze P, Langlais B, Macmillan S, Mandea M, Merayo J, Newitt L, Purucker M, Risbo T, Stampe M, Thomson A, Voorhies C (2000) Oersted initial field model. Geophys Res Lett 27:3607–3610

Olson P (2002) The disappearing dipole. Nature 416:590–591

Olson P (2003) Thermal interaction of the core and mantle. In: Jones CA, Soward AM, Zhang K (eds) Earth's core and lower mantle. Taylor and Francis, London

Olson P, Christensen U, Glatzmaier GA (1999) Numerical modeling of the geodynamo: mechanisms of field generation and equilibration. J Geophys Res 104:10383–10404

Olson P, Sumita I, Aurnou J (2002) Diffusive magnetic images of upwelling patterns in the core. J Geophys Res 107(12). DOI 10.1029/2001jb000384

Pais A, Hulot G (2000) Length of day decade variations, torsional oscillations and inner core superrotation: evidence from recovered core surface zonal flows. Phys Earth Planet Inter 118:291–316

Pan Y, Hill MJ, Zhu R, Shaw J (2004) Further evidence for low intensity of the geomagnetic field during the early Cretaceous time: using the modified Shaw method and microwave technique. Geophys J Int 157:553–564

Phillips JB (1996) Magnetic navigation. J Theor Biol 180:309–319

Pinto OJ, Gonzalez WD, Pinto IRC, Gonzalez ALC, Mendes OJ (1992) The South Atlantic magnetic anomaly: three decades of research. J Atmos Terr Phys 54:1129–1134

Poirier JP (1994) Physical properties of the Earth's core. CR Acad Sci Paris 318:341–350

Poirier JP (2000) Introduction to the physics of the Earth's interior. Cambridge University Press, Cambridge

Raup DM (1985) Magnetic reversals and mass extinctions. Nature 314:341–343

Roberts PH, Glatzmaier GA (2000) Geodynamo theory and simulations. Rev Mod Phys 72:1081–1123

Roberts PH, Scott S (1965) On analysis of the secular variation. J Geomagn Geoelectr 17:137–151

Sabaka TJ, Olsen N, Langel RA (2002) A comprehensive model of the quiet time, near-earth magnetic field: phase 3. Geophys J Int 151:32–68

Sabaka TJ, Olsen N, Purucker M (2004) Extending comprehensive models of the Earth's magnetic field with Oersted and CHAMP. Geophys J Int 159(2):521–547

Sarson GR, Jones CA (1999) A convection driven geodynamo reversal model. Phys Earth Planet Inter 111:3–20

Schubert G, Turcotte DL, Olson P (2001) Mantle convection in the Earth and planets. Cambridge University Press, Cambridge

Secco RA, Schloessin HH (1989) The electrical resistivity of solid and liquid Fe at pressures up to 7 GPa. J Geophys Res 94: 5887–5894

Selkin PA, Tauxe L (2000) Long-term variations in palaeointensity. Philos Trans R Soc Lond A 358:1065–1088

Simitev R, Busse FH (2005) Prandtl-number dependence of convection-driven dynamos in rotating spherical fluid shells. J Fluid Mech 532:365–388

Sisco GL, Chen CK (1975) The paleomagnetosphere. J Geophys Res 80:4675–4680

Stacey FD (1992) Physics of the Earth, 3rd edn. Brookfield Press, Brisbane, AU

Stevenson DJ (1987) Limits on lateral density and velocity variations in the Earth's outer core. Geophys J R Astron Soc 88:311–319

Stevenson DJ (1990) Fluid dynamics of core formation. In: Newsom HE, Jones JH (eds) Origin of the Earth. Oxford University Press, London, UK, pp 231–249

Takahashi F, Matsushima M, Honkura Y (2005) Simulations of a quasi-Taylor state geomagnetic field including polarity reversals on the Earth simulator. Science 309:459–461

Tanaka H, Kono M, Uchimura H (1995) Some global features of paleointensity in geologic time. Geophys J Int 120:97–102

Tarduno JA, Cotrell RD, Smirnov AV (2001) High geomagnetic intensity during the mid-Cretaceous from Thellier analyses of single plagioclase crystals. Science 291:1779–1783

Thouveny N, Creer KM, Williamson D (1993) Geomagnetic moment variations in the last 70,000 years, impact on production of cosmogenic isotopes. Palaeogeogr Palaeoclimatol Palaeoecol 7:157–172

Valet JP (2003) Time variations in geomagnetic intensity. Rev Geophys 41(1):1004. DOI 10.1029/2001RG000104

Valet J-P, Meynadier L, Guyodo Y (2005) Geomagnetic dipole strength and reversal rate over the past two million years. Nature 435:802–805

Verosub KL, Cox A (1971) Changes in the total geomagnetic energy external to Earth's core. J Geomagn Geoelectr 23:235–242

Voorhies CV (1986) Steady flows at the top of Earth's core derived from geomagnetic field models. J Geophys Res 91:12444–12466

Walker MM, Dennis TE, Kirschvink JL (2002) The magnetic sense and its use in long-distance navigation by animals. Curr Opin Neurobiol 12:735–744

Whaler KA, Davis RG (1997) Probing the Earth's core with geomagnetism. In: Crossley DJ (ed) Earth's deep interior. Gordon and Breach, Amsterdam, pp 114–166

Wicht J, Olson P (2004) A detailed study of the polarity reversal mechanism in a numerical dynamo model. Geochem Geophys Geosyst 5(3). DOI 10.1029/2003GC000602

Wood BJ, Halliday AN (2005) Cooling of the Earth and core formation after the giant impact. Nature 437:1345–1348

Yamamoto Y, Tsunakawa H (2005) Geomagnetic field intensity during the last 5 Myr: LTD-DHT Shaw palaeointensities from volcanic rocks of the Society Islands, French Polynesia. Geophys J Int 162:79–114

Yang S, Odah H, Shaw J (2000) Variations in the geomagnetic dipole moment over the last 12,000 years. Geophys J Int 140: 158–162

Yokoyama Y, Yamazaki T (2000) Geomagnetic paleointensity variation with a 100 kyr quasi-period. Earth Planet Sci Lett 181:7–14

Yoshihara A, Hamano Y (2000) Intensity of the Earth's magnetic field in late Archean obtained from diabase dikes of the Slave Province, Canada. Phys Earth Planet Inter 117:295–307

Yukutake T (1967) The westward drift of the Earth's magnetic field in historic times. J Geomagn Geoelectr 19:103–116

Zhang K, Busse FH (1989) Convection driven magnetohydrodynamic dynamos in rotating spherical shells. Geophys Astrophys Fluid Dyn 49:97–116

Zhu RX, Pan YX, Shaw J, Li DM, Li Q (2001) Paleointensity just prior to the Cretaceous normal superchron. Phys Earth Planet Inter 128:207–222